LITHIUM-ION BATTERY MODELING FOR ELECTRIC VEHICLES AND REGENERATIVE CELL TESTING PLATFORM

by

Andishe Moshirvaziri

A thesis submitted in conformity with the requirements
for the degree of Master of Applied Science
Graduate Department of Electrical and Computer Engineering
University of Toronto

Abstract

LITHIUM-ION BATTERY MODELING for ELECTRIC VEHICLES and REGENERATIVE CELL TESTING PLATFORM

Andishe Moshirvaziri
Master of Applied Science
Graduate Department of Electrical and Computer Engineering
University of Toronto
2013

Electric Vehicles (EVs) have gained acceptance as low or zero emission means of transportation. This thesis deals with the design of a battery cell testing platform and Lithium-Ion (Li-Ion) battery modeling for EVs. A novel regenerative cell testing platform is developed for cell cycling applications. A 300 W - 5 V cell cycler consisting of a buck and a boost converter is designed.

Furthermore, a novel battery modeling approach is proposed to accurately predict the battery performance by dynamically updating the model parameters based on the battery temperature and State of Charge (SOC). The comparison between the experimental and the model simulation results of an automotive cell under real-world drive-cycle illustrates 96.5% accuracy of the model. In addition, the model can be utilized to assess the long-term impact of battery impedance on performance of EVs under real-world drive-cycles.

Acknowledgements

First and foremost, I would like to express my sincere gratitude to my supervisor, Professor Olivier Trescases, whose support, direction, guidance and encouragement made it possible for this thesis to see the light of this day. His help and patience during my research made it possible for me to push the boundaries of my own knowledge and help gain the understanding which I currently have. His encouraging words throughout my research motivated and kept me going which was invaluable to my thesis.

I would like to thank Roger Gerson and Paul Daniel from Brammo Inc. who not only supported this project financially, but also provided invaluable guidance, critical data and the required resources. Their help and support were integrals to the success of this thesis and I highly appreciate their efforts.

I would also like to thank my brother and colleague, Mazhar Moshirvaziri, who helped and guided me throughout my graduate degree. He has been my life long mentor and has helped me through many challenges including my thesis. I wish him success in all his future endeavors. I would also like to thank my friends and colleagues in the Energy Systems group for providing me support to overcome some of the obstacles. Shahab Poshtkouhi who on many occasions was the sounding board for my ideas. Behzad Mahdavikhah helped me solve some problems associated to my project. I wish them both success in pursuing their PhD studies. I am very grateful to Farhad Yahyaie and Kia Filsoof for their support. I would also like to extend my gratitude to my undergraduate student assistants, Yajneshvar Arumugam and Jackycy Liu, who assisted me in the experimental parts of my project. Last but most importantly, I would like to thank my family who have provided me with unconditional love and support throughout my life. My parents who supported my ideas from the start and encouraged me to always reach for the stars. I learned from them that hard work and patience pays off if you are focused on your goal. My older brother, Reza, and my sister, Khazal, who were a constant voice of support and encouragement for me. Also, my nephew, Sadra, who kept me laughing

and smiling throughout my studies.

I would like to end my acknowledgement by quoting a good friend of mine, Maz Alam, who when saw me stressed often said ”Whatever doesn’t kill you makes you stronger”. I thank him for all the support and encouragement he provided me.

Contents

List of Tables

List of Figures

Chapter 1

Introduction

1.1 Modern Electric Vehicles

During the past few decades, the atmospheric CO_2 concentration has dramatically increased resulting in global warming and significant climate change [1,2]. The global price of crude oil is predicted to significantly increase by 2035 [3]. Therefore, the ownership cost of Internal Combustion Engine (ICE) vehicles continue to increase, which is paving the way for alternative technologies such as EVs. EVs have gained acceptance as low or zero emission means of transportation. The energy required by EVs can be supplied by clean renewable energy sources in the future [4,5]. In addition, EVs have the ability to recover energy that otherwise would be lost during braking, known as Regenerative (Regen) braking [6–9].

Off-grid, battery powered EVs can be categorized based on the power level [10],

1. Light electrical vehicles (LEV) such as electrical bikes, scooters and motorcycles with a power demand of less than several kilowatts,

2. Sedan vehicles, which includes sedan hybrid electrical vehicles (HEV) and full electrical vehicles up to 100 kW and

3. Heavy-duty vehicles which are used for public transportation such as buses, with a power level over 100 kW.

Among various Energy Storage Systems (ESS) such as capacitors and flywheels, electrochemical batteries are preferred in EVs due to their superior energy density [6, 11].

1.1.1 Challenges in Electric Vehicles

Currently, EVs face multiple challenges which are the prohibiting factors for mass deployment and commercialization. High initial costs, limited lifetime and relatively poor performance at low temperature are often cited as the most important issues, with the latter three directly involving the ESS and BMS of the vehicle [12–15].

The average lifetime of batteries (typically defined by a 20% degradation in battery capacity) in EVs is approximately 8 to 10 years [13]. In practice, the lifetime of the battery is reduced due to the high power profile of the vehicle during acceleration and braking, which can be much more than 10× higher than the average power. An example of a power demand of an electric bicycle [6] in an urban driving environment is shown in Fig. 1.1. The LEV spends a fair amount of time in low power and idle modes, however, it experiences some high power peaks frequently. Driving behavior, recharging habits, depth of discharge (DOD) and ambient temperature are other factors which impact the lifetime of the batteries by varying degrees. Analyzing the effects of these factors can improve the capability of battery models in both performance and lifetime prediction [13, 16].

In this project, a platform is designed and implemented to analyze the effects of average discharge current, ambient temperature and drive cycle dynamics. Prior to discussing the above mentioned platform and its analysis, it is essential to have an overview of batteries, common EV battery chemistries and their associated challenges.

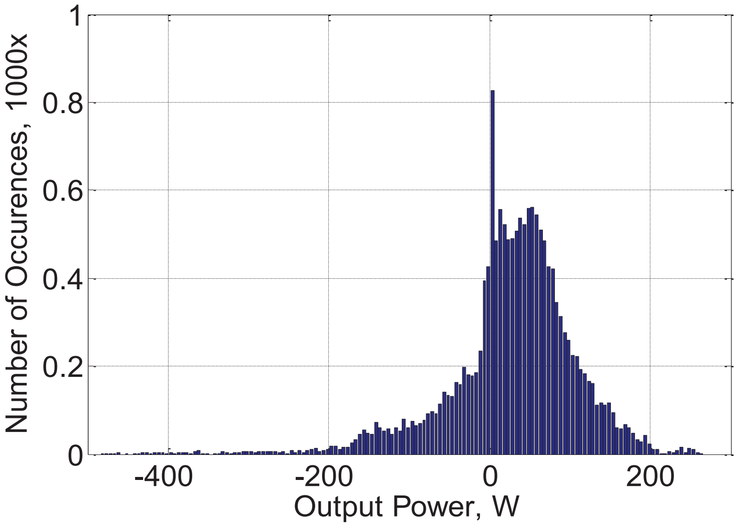

Figure 1.1: Power demand histogram for an LEV [6].

1.2 Batteries

1.2.1 Elements and Specification of Batteries

A battery is an energy storage device that converts the chemical energy stored in its active materials into electrical energy by means of electrochemical reactions. The basic electrochemical storage element is a cell. A battery consists of one or more cells, connected in series, parallel or both, based on the desired nominal battery voltage and capacity. A cell system can be described using three main components:

1. Anode

   The chemical reaction at the anode (oxidation) releases electrons that flow to the cathode through an external circuit. The anode material is selected based on its efficiency, high specific capacity, conductivity, stability, ease of fabrication and low cost.

2. Cathode

   The chemical reaction at the cathode (reduction) accepts the electrons. The cathode is selected based on its voltage and chemical stability over time.

3. **Electrolyte**

   The electrolyte completes the cell circuit by transporting the ions. The electrolyte can be liquid, like water, acids, alkalis or solvents with dissolved salts. The electrolyte can be selected based on its high conductivity, non-reactivity with the electrode materials, stability in properties at various temperatures, safety and cost.

Physically, the electrodes are electronically isolated preventing internal short-circuit situations, however, they are surrounded by the electrolyte. In a practical cell design, separators which are permeable to the electrolyte are used to provide mechanical separation between the electrodes [17]. The most beneficial combination of all these elements are those which result in a cell with light weight, high voltage and high capacity [1].

When a cell is discharging, electrons extracted from oxidation at the anode electrode flow to the cathode electrode where reduction happens. During the charging process, the current flow is reversed [18]. The charge and discharge process is shown in Fig. 1.2.

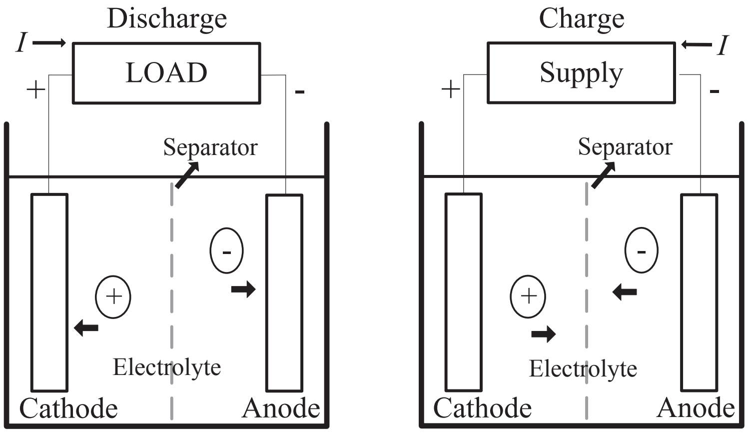

Figure 1.2: Electrochemical operation in a cell.

When chemical reactions happen in a cell, the free energy of the system decreases due to its transformation into electrical energy. The theoretical cell voltage is a function of the property of the materials and is the sum of the anode and cathode potentials. The theoretical capacity is a function of the amount of active materials used in the cell.

1.2.2 Common Battery Chemistries

In this section, a summary of common available battery chemistries, their advantages and disadvantages are provided.

1. Lead-Acid

   The three main elements of Lead-Acid batteries are Lead, Lead Oxide and diluted Sulfuric Acid. Low cost and mature technology are some of the advantages, however, self discharge, heavy weight, low specific power and energy due to the heavy lead collectors, limited life cycle are the main disadvantages of this chemistry [19, 20].

2. Nickel

   Nickel Metal Hydride (NiMH) and Nickel Cadmium (NiCad) are the most popular Nickel based battery technologies. NiMH batteries have advanced performance in safety and power density. The Fluctuating price of Nickel [21,22] and its low energy density as compared to Lithium-Ion batteries are the main poor characteristics of this battery technology. However, NiMH is still the most commonly used battery technology used in EVs [23]. NiCad technology has the most stable performance (its performance is not even affected by over-charged or over-discharged over time [24]). However, as this chemistry contains poisonous Cadmium, it is banned for industry applications in many countries [6, 23].

3. Lithium-Ion

   The common materials used for the positive electrode of Lithium-Ion (Li-Ion) batteries are Cobalt Oxide, Manganese Oxide, Iron Phosphate, Nickel Manganese Cobalt Oxide and Nickel Cobalt Aluminum Oxide. Lithium salt in organic solvent and carbon are used for the negative electrode and electrolyte, respectively. Lithium-based batteries offer higher specific energy than Lead-Acid and Nickel-based batteries [6, 23], as shown in Table 1.1. Due to the high specific energy (over

100 Wh/kg), recyclability and long cycle life (several thousand cycles) [25], Li-Ion batteries units are produced in billions every year in the market of popular devices such as laptops, cell phones and cameras [1].

There are four main Li-Ion battery chemistries [6, 23]:

(a) Lithium Cobalt

Lithium Cobalt Oxide (Li-Co Oxide) batteries provide advanced electrical performance and more specifically, very high specific energy. However, they suffer from poor thermal stability. This characteristic limits the applications of this technology to few industries such as laptops, cell phones and other personal electronic devices. As of this writing, this chemistry is not suitable for industrial applications and electric vehicles due to safety issues [23].

(b) Lithium Manganese

Lithium Manganese Oxide (Li-Mn Oxide) offers higher safety factors and lower cost than Lithium Cobalt, however, it has a fairly short life cycle. Therefore, it is limited to low power technologies like electrical bicycles and scooters [23].

(c) Lithium Ferro Phosphate

Lithium Ferro Phosphate (Li-Fe Phosphate) provides a good balance in safety, life cycle and cost. However, its energy density is lower than other lithium chemistries [23].

(d) Lithium Nickel Manganese Cobalt Oxide

Lithium Nickel Manganese Cobalt Oxide (Li-Ni-Mn-Co Oxide) was developed as an alternative to Li-Co Oxide to balance the cost and performance of the battery [26].

The characteristics of common Li-Ion chemistries are illustrated in Fig. 1.3. Li-Ni-Mn-Co Oxide battery is a suitable choice for EVs [27], as it offers an excellent trade-off between safety, capacity and performance [26].

As of this writing, Li-Ion chemistry with its superior specific energy, power and voltage range is considered the most suitable candidate among other chemistries for EVs [10, 13, 28] and is the main focus of this work.

Table 1.1: Specific-Energy of Different Battery Chemistries [6]

	Lead-Acid	Ni-Cd	Ni-MH	Li-Fe Phosphate	Li-Mn Oxide	Li-Ni-Mn Co Oxide	Li-Co Oxide
Typical Specific Energy (Wh/kg)	40	60	90	110	120	140	170

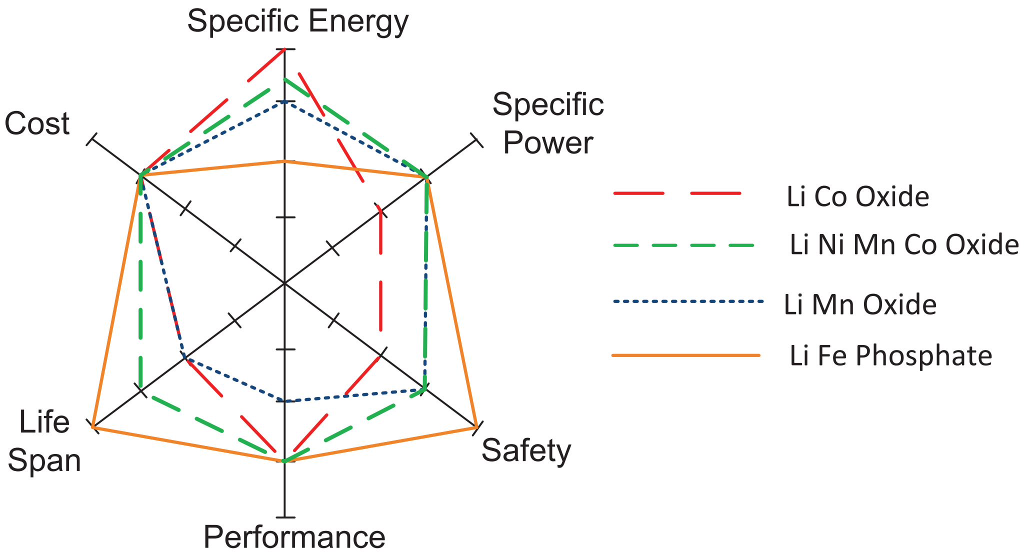

Figure 1.3: Characteristic comparison of different Lithium based technologies [6].

1.2.3 Challenges of Li-Ion Battery Technology in EVs

Li-Ion technology must be improved in terms of costs and lifetime to improve the large scale adoption of EVs [29]. Prediction and extension of the battery pack lifetime plays an important role in the EV market [16]. The two main challenges of Li-Ion battery technology in EVs are:

1. Capacity Fade

   Carbonaceous materials used in all Li-Ion batteries [30], are known to have dominant effects in the capacity loss at high discharge rates [31]. Among the various carbonaceous materials, natural graphite is the most attractive choice as it has a high theoretical capacity, abundance and low cost. During the cell operation, non-reversible chemical reactions on the surface of graphite happen among Lithium ions, solvents and electrons. The by-products of these reactions, accumulate and form a surface film on the carbon electrode known as Solid Electrolyte Interface (SEI). A Battery can stop performing when the Lithium ions can no longer pass the SEI layer due to its thickness. Therefore, lifetime and cyclability of a cell depends on its SEI layer [30].

   Capacity fade of Lithium-ion batteries depends on the various factors such as average discharge current and temperature of the cell. As demonstrated in [10, 31], capacity fade is proportional to the average discharge rate. If a battery discharges with a high current, the internal cell temperature increases due to the electrical loss inside the battery. The electrical loss inside a battery is approximated as:

   $$P_{loss} \quad = \quad R_{bt} \times I_{bt}^2, \tag{1.1}$$

   where I_{bt} is the average battery current, R_{bt} is the Equivalent Series Resistance (ESR) of the battery, and P_{loss} is the power loss inside the battery. The internal cell temperature can not be directly measured as it is impractical. The difference between ambient temperature and cell temperature can be as high as 60 degree during high discharge rates. High current and high temperature can increase the speed of chemical reactions and the formation of the SEI layer.

Ambient temperature is another important factor that affects the performance and the lifetime of batteries. Li-Ion batteries have better performance at higher temperature as the chemical reactions proceed faster. However, higher temperature accelerates the capacity fade in Lithium-ion batteries [10].

Although the effect of average current, DOD and ambient temperature on capacity fade of Li-Ion batteries is widely studied, there is very limited research that investigates the impact of real-world dynamic drive-cycles on capacity fade of Li-Ion batteries, especially at low ambient temperature.

2. Performance

A general EV architecture consists of a battery pack, BMS, bi-directional inverter, controller and traction motor as shown in Fig. 1.4. The battery packs deployed for EVs consist of several battery modules connected in series, and each module is a combination of numerous battery cells. In practice, battery cells in a module are not identical which limits the battery performance (in this thesis, the battery performance is defined as the calculated cumulative deliverable energy). This can be mitigated using cell balancing techniques which are performed by the BMS. The BMS is required for safe operation of the battery pack as well as better performance of the EV [12, 14, 15]. The central BMS typically communicates with the inverter using the Controller Area Network (CAN) protocol [6, 14].

During the vehicle operation, the driver indirectly controls the motor torque through the acceleration or brake pedals. In addition, the BMS system broadcasts the allowable battery current range in real time based on an internal battery model. The inverter saturates the current in the torque control loop based on the allowable range. When the vehicle accelerates, the requested torque and battery current (I_{bt}) are positive, and the battery is discharges. During Regen braking, the requested torque is negative, therefore, the battery charges which means the battery current is positive.

During the vehicle operation, the main BMS utilizes a battery model to estimate the maximum and minimum allowable current of the battery pack based on the operating conditions. If the required battery current is outside of the allowable range, the motor current (I_{motor}) is saturated to limit the battery current. The controller sends the PWM signals to the inverter to regulate I_{motor} to the reference value. In failure situations (such as short circuit situations in cell or module level) the controller can either set the maximum allowable battery current to zero or open the contactor directly.

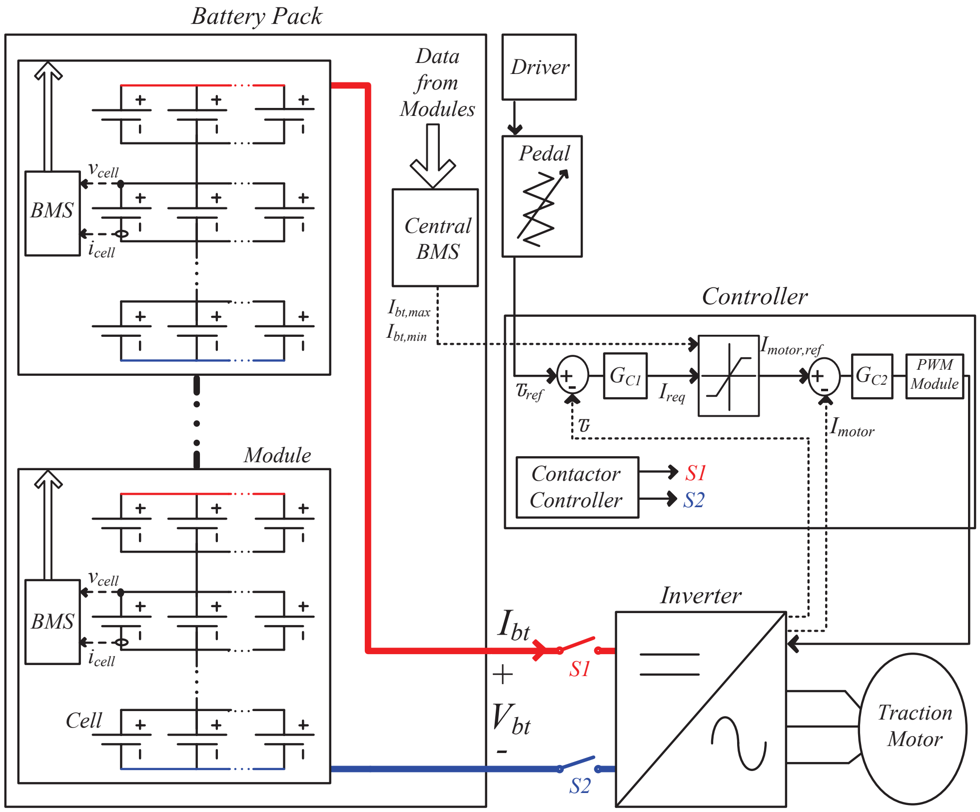

Figure 1.4: Electric vehicle architecture.

A simple battery model is shown in Fig. 1.5, where the battery terminal voltage (V_{bt}) can be calculated based on the open-circuit voltage (V_{oc}), internal impedance (Z) and I_{bt} using the

$$V_{bt} = V_{OC} - Z \times I_{bt}. \tag{1.2}$$

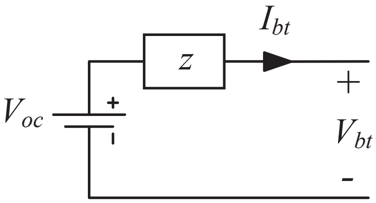

Figure 1.5: Simple battery model used to predict dynamic voltage drops at V_{bt}.

For battery safety, if V_{bt} drops below the minimum battery voltage (under-voltage situation) or rises above the maximum battery voltage (over-voltage situation), the BMS broadcasts a zero available current and the inverter is unable to drive the motor. An under-voltage fault may occur when the BMS overestimates the allowable discharging current, and the battery voltage drops below the minimum voltage. Over-voltage situation can happen when the BMS overestimates the allowable charging current during the Regen braking, and the battery voltage rises above the maximum voltage. Therefore, it is critical for the BMS to accurately predict the allowable battery current range, which is only possible by providing the BMS with a precise battery model.

1.3 Thesis Motivation and Objectives

The goal of this work is to design a cell testing platform and battery modeling for electric vehicles. More specifically, a novel cell testing platform is designed as a powerful tool to investigate the long-term capacity fade of Li-Ion batteries. Furthermore, a novel battery modeling approach is proposed to accurately predict the battery performance. The proposed model is intended to be implemented in real-time BMS systems to further improve the vehicle performance.

Although commercialized battery cell testers can be utilized to test batteries, they are not ideal for this work as high power automotive grade cells are used which would lead to large amount of wasted energy. Assuming the use of a commercialized six-channel cycler, the amount of energy wasted would be 350 kWh in one year, hence, high power cooling systems are required. The first objective of this thesis is to design a multi-channel Li-Ion cell testing platform having the following requirements:

- A modular architecture with fully independent channels,
- A low cost, low volume and digitally-controlled design with a switching frequency of 200 kHz,
- A regenerative design for transmitting the battery energy to power grid during discharging, and
- A power level of 300 W and input voltage of 5 V per channel corresponding to a single Li-Ion cell.

Ultra-capacitors are exploited as the auxiliary storage elements in the system to maximize the efficiency and stability by storing the instantaneous battery current (with high dynamics) while the average battery energy is transmitted to the power grid by the inverter.

The second objective is to propose a battery modeling approach which dynamically updates the model parameters based on battery temperature and SOC variations. The model considers the following factors:

- State of Charge
- Cell and ambient temperature
- Self heating
- Simplicity for digital real-time implementation in an embedded system.

Furthermore, the designed battery model is used to illustrate the effects of battery impedance on the performance of EVs under experimental drive-cycles based on real driving conditions. This thesis is organized as follows, Chapter 2 introduces the programable and regenerative multi-channel Li-Ion cell testing platform. A cycler with a novel design, control strategy, implementation and experimental results are provided. In Chapter 3, a battery modeling approach is proposed which can dynamically update the model parameters based on battery temperature and SOC. The model parameters are experimentally extracted for two different automotive grade cells. Utilizing the proposed modeling approach, the impact of battery impedance on performance of EVs under real-world drive-cycles is discussed in Chapter 4. Finally, the conclusion and future work are covered in Chapter 5.

References

[1] B. Scrosati and J. Garche, “Lithium batteries: Status, prospects and future,” *Journal of Power Sources*, vol. 195, no. 9, pp. 2419 – 2430, 2010.

[2] N. Omar, P. Van den Bossche, G. Mulder, M. Daowd, J. Timmermans, J. Van Mierlo, and S. Pauwels, “Assessment of performance of lithium iron phosphate oxide, nickel manganese cobalt oxide and nickel cobalt aluminum oxide based cells for using in plug-in battery electric vehicle applications,” in *Vehicle Power and Propulsion Conference (VPPC), 2011 IEEE*, pp. 1–7, 2011.

[3] United States Energy Information Administration (EIA). Accessed in August 2012, available at http://www.eia.gov/.

[4] X. Li, L. A. C. Lopes, and S. Williamson, “On the suitability of plug-in hybrid electric vehicle (phev) charging infrastructures based on wind and solar energy,” in *Power Energy Society General Meeting, 2009. PES ’09. IEEE*, pp. 1–8, 2009.

[5] Z. Li and A. Khaligh, “An integrated parallel synchronous rectifier and bi-directional dc/dc converter system for solar and wind powered hybrid electric vehicle,” in *Industrial Electronics, 2009. IECON ’09. 35th Annual Conference of IEEE*, pp. 3779–3784, 2009.

[6] M. Moshirvaziri, “Ultracapacitor/battery hybrid energy storage systems for electric vehicles,” Master’s thesis, University of Toronto, Canada, 2012.

[7] R. H. Miller, J. J. Brockman, and A. Kusko, "Regeneration in electric vehicles," in *Vehicular Technology Conference, 1978. 28th IEEE*, vol. 28, pp. 156–156, 1978.

[8] M. Montazeri-Gh, M. Soleymani, and S. Hashemi, "Impact of traffic conditions on the active suspension energy regeneration in hybrid electric vehicles," *Industrial Electronics, IEEE Transactions on*, vol. 60, no. 10, pp. 4546–4553, 2013.

[9] M.-J. Yang, H.-L. Jhou, B.-Y. Ma, and K.-K. Shyu, "A cost-effective method of electric brake with energy regeneration for electric vehicles," *Industrial Electronics, IEEE Transactions on*, vol. 56, no. 6, pp. 2203–2212, 2009.

[10] E. Prada, D. Di Domenico, Y. Creff, J. Bernard, V. Sauvant-Moynot, and F. Huet, "Physics-based modelling of lifepo4-graphite li-ion batteries for power and capacity fade predictions: Application to calendar aging of phev and ev," in *Vehicle Power and Propulsion Conference (VPPC), 2012 IEEE*, pp. 301–308, 2012.

[11] F. Werfel, U. Floegel-Delor, T. Riedel, R. Rothfeld, D. Wippich, B. Goebel, G. Reiner, and N. Wehlau, "A compact hts 5 kwh/250 kw flywheel energy storage system," *Applied Superconductivity, IEEE Transactions on*, vol. 17, no. 2, pp. 2138–2141, 2007.

[12] A. Eddahech, O. Briat, and J. Vinassa, "Real-time soc and soh estimation for ev li-ion cell using online parameters identification," in *Energy Conversion Congress and Exposition (ECCE), 2012 IEEE*, pp. 4501–4505, 2012.

[13] J. Shen, S. Dusmez, and A. Khaligh, "An advanced electro-thermal cycle-lifetime estimation model for lifepo4 batteries," in *Transportation Electrification Conference and Expo (ITEC), 2013 IEEE*, pp. 1–6, 2013.

[14] J. Yan, C. Li, G. Xu, and Y. Xu, "A novel on-line self-learning state-of-charge estimation of battery management system for hybrid electric vehicle," in *Intelligent Vehicles Symposium, 2009 IEEE*, pp. 1161–1166, 2009.

[15] A. Hentunen, T. Lehmuspelto, and J. Suomela, "Electrical battery model for dynamic simulations of hybrid electric vehicles," in *Vehicle Power and Propulsion Conference (VPPC), 2011 IEEE*, pp. 1–6, 2011.

[16] R. Dougal, S. Liu, and R. White, "Power and life extension of battery-ultracapacitor hybrids," *Components and Packaging Technologies, IEEE Transactions on*, vol. 25, no. 1, pp. 120–131, 2002.

[17] T. B. Reddy and D. Linden, *Linden's Handbook of Batteries, 4th Ed.* 2011.

[18] W. Luo, C. Lv, L. Wang, and C. Liu, "Study on impedance model of li-ion battery," in *Industrial Electronics and Applications (ICIEA), 2011 6th IEEE Conference on*, pp. 1943–1947, 2011.

[19] D. Edwards and C. Kinney, "Advanced lead acid battery designs for hybrid electric vehicles," in *The Sixteenth Annual Battery Conference on Applications and Advances*, pp. 207 –212, 2001.

[20] A. Cooper and P. Moseley, "Progress in the development of lead-acid batteries for hybrid electric vehicles," in *IEEE Vehicle Power and Propulsion Conference, VPPC*, pp. 1 –6, Sept. 2006.

[21] "5 year nickel prices and price charts." InfoMine, Commodity Prices. Accessed in September 2013, available at http://www.infomine.com/.

[22] "1 year nickel spot chart." KITCO, Historical Charts. Accessed in September 2013, available at http://www.kitcometals.com/.

[23] K. Yiu, "Battery technologies for electric vehicles and other green industrial projects," in *Power Electronics Systems and Applications (PESA), 2011 4th International Conference on*, 2011.

[24] "Portable rechargeable batteries (secondary batteries)." Battery Association of Japan, About Batteries. Accessed in September 2013, available at http://www.baj.or.jp/e/knowledge/history03.html.

[25] S. G. Chalk and J. F. Miller, "Key challenges and recent progress in batteries, fuel cells, and hydrogen storage for clean energy systems," *Journal of Power Sources*, vol. 159, no. 1, pp. 73 – 80, 2006.

[26] "Li(nmc)o2 - lithium nickel manganese cobalt dioxide." umicore Cobalt and Specialty Materials. Accessed in Agust 2013, available at http://csm.umicore.com/products/rechargeableBatteriesMaterials/lithiumNmcDioxide/.

[27] "Learn about batteries." Battery University. Accessed July 2012, available at http://batteryuniversity.com/learn/article/types_of_lithium_ion.

[28] A. Baba and S. Adachi, "State of charge estimation of lithium-ion battery using kalman filters," in *Control Applications (CCA), 2012 IEEE International Conference on*, pp. 409–414, 2012.

[29] J. Miller, T. Bohn, T. Dougherty, and U. Deshpande, "Why hybridization of energy storage is essential for future hybrid, plug-in and battery electric vehicles," in *Energy Conversion Congress and Exposition, 2009. ECCE 2009. IEEE*, pp. 2614–2620, 2009.

[30] J. S. Gnanaraj, R. W. Thompson, S. N. Iaconatti, J. F. DiCarlo, and K. M. Abraham, "Formation and growth of surface films on graphitic anode materials for li-ion batteries," *Electrochemical and Solid-State Letters*, vol. 8, no. 2, pp. A128–A132, 2005.

[31] G. Ning, B. Haran, and B. N. Popov, "Capacity fade study of lithium-ion batteries cycled at high discharge rates," *Journal of Power Sources*, vol. 117, pp. 160–169, May 2003.

Chapter 2

Multi-Channel Cell Testing Platform

2.1 Introduction

The focus of this chapter is the design of a programmable and regenerative multi-channel Li-Ion cell testing platform as a powerful tool to investigate the long-term effects of ambient temperature, average current and current dynamics on the lifetime of Li-Ion batteries.

The Li-Ion cells used in this project are provided by Brammo Inc. [1]. The cell specifications are listed in Table 2.1. The nominal cell capacity and voltage are 10 Ah and 3.7 V, respectively. The maximum continuous discharge current can be as high as 5 C (50 A), however, the battery cell can deliver 8 C (constant discharge) for 15 seconds. The cell capacity is rated to reduce by a maximum of 10% after 500 cycles.

The designed cell cycler platform consists of six parallel channels in order to test the batteries in various scenarios, as shown in Table 2.2. The channels are capable of tracking dynamic currents up to 8 A/ms. Two sets of drive-cycle data, representing urban and freeway drive-cycles, are available from a commercialized motorcycle provided by Brammo Inc.. The current profiles of the urban and freeway drive-cycles are shown in Fig. 2.1.

Table 2.1: Li-Ion Cell Specifications

Item	Value
Rated Capacity	10 – 10.5 Ah
Nominal Voltage	3.7 V
Charged Limited Voltage	4.2 V
Discharge $cut-off$ Voltage	3.0 V
Internal Impedance	3.5±1 mΩ (at 1 kHz at 25 ± 5°C)
Standard Charge	Constant Current: 0.2 C Constant Voltage: 4.2 V End-of-charge Current: 500 mA
Standard Discharge	Constant Current: 0.2 C to Discharge cut-off voltage
Maximum Continuous Charge Current	1 C (10 A)
Maximum Continuous Discharge Current	5 C (50 A)
Maximum Discharge Current	8 C (80 A) for 15 seconds
Operating Temperature	Charge: 0 – 45°C Discharge: (−10) – 55°C

Table 2.2: Cycling Plan.

Channel Number	Discharge Mode	Ambient Temperature (°C)	Average C Rate	Peak C Rate	Duration (min)
1	constant C-rate	25	1	1	60
2	constant C-rate	25	2	2	30
3	constant C-rate	15	2	2	30
4	constant C-rate	25	3.5	3.5	17
5	Urban Drive	25	1	3.5	5
6	Freeway Drive	25	2	4	2

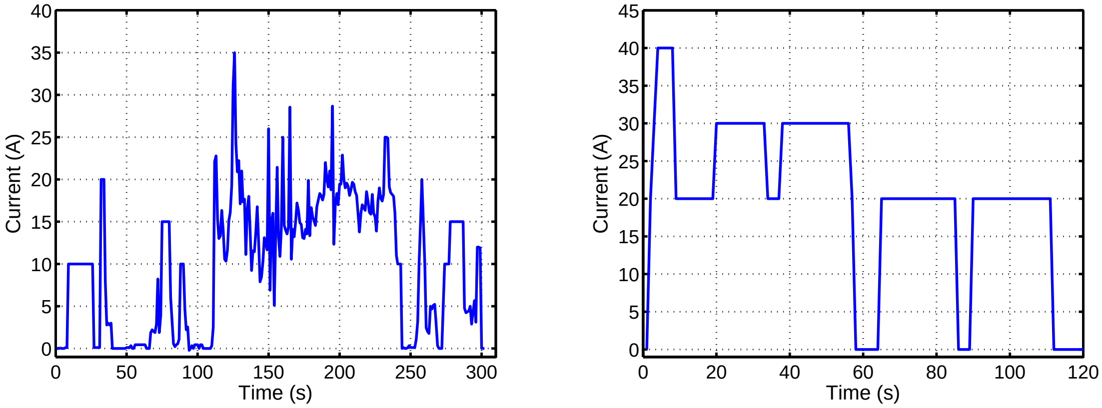

(a) (b)

Figure 2.1: Sample current profiles for the (a) urban and (b) freeway drive-cycle.

There are two key reasons that the proposed cell cycler, rather than the industrial [2,3] and other cell cyclers, is uniquely suited to this application.

1. The resistive load based industrial testers are not ideal for this application as the tests would run continuously for months which would lead to a large amount of wasted power for the high power battery cells used in this work. Therefore, a regenerative cycler which transfers the power of the cells to the grid, is required [2,3].
2. The architectures shown in Fig. 2.2(a) with a bi-directional inverter [4–6] and Fig. 2.2(b) with a uni-directional inverter are potential candidates which can overcome the above mentioned challenges. However, they fail to follow the required current profiles based on the cell voltage and current level (3.7 V - 80 A).

2.2 System Design

The proposed regenerative cell cycler utilizes an inverter to send the battery power to the grid as shown in Fig. 2.3. The cycler system can be programmed by the user to follow the desired battery current command. The cell cycler is designed to be modular by using off-the-shelf components which provides expansion flexibility to the platform.

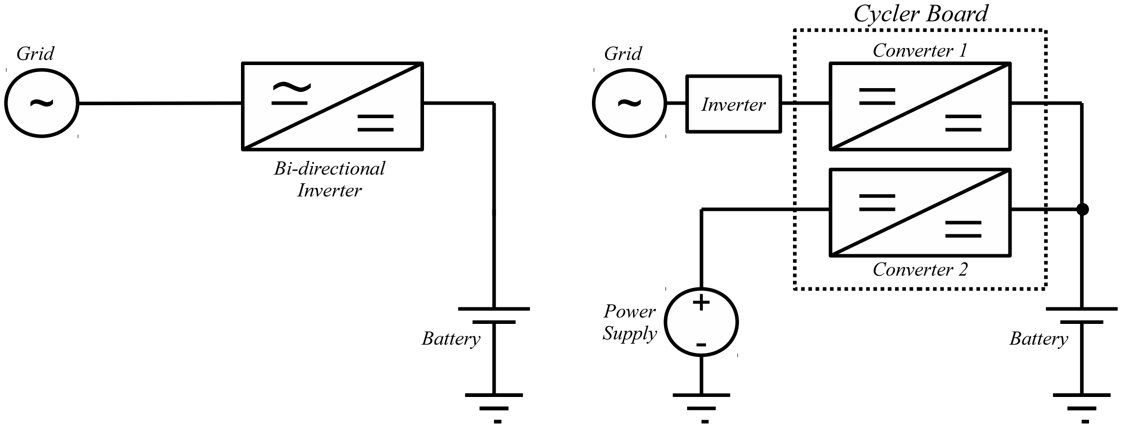

(a) (b)

Figure 2.2: (a) Bi-directional and (b) uni-directional inverter-based regenerative cell cycler architectures.

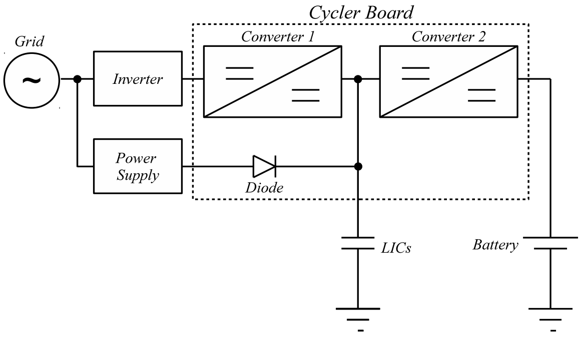

(a)

Figure 2.3: Proposed cell cycler architecture.

In the proposed cell cycler, the battery is connected to the main bus using a bi-directional dc-dc converter, which in turn is connected to the inverter by a second converter. The Li-Ion Capacitors (LICs) with high power density (7 kW/kg), high cycling ability and low ESR (1 mω) are added to the system as short-term energy storage elements to stabilize the system by reducing the current stress on the inverter. The LICs store the instantaneous battery current (with high dynamics) while the average stored energy in LICs is transferred to the inverter through the second converter.

The descriptions of the components are as follows:

1. Power Supply

An off-the-shelf 6 V current-limited dc power supply is used to power the controller module of the cycler board and to charge the battery. A diode is connected in series with the power supply to protect it from reverse current flow. In order to minimize the conduction loss, a diode is selected which has the minimum voltage drop over the operating current range.

2. Lithium-Ion Capacitor

Ultra-capacitors are used as short-term energy storage for power smoothing and stabilizing the system. Electrochemical Double-Layer Capacitors (EDLC), also known as ultra-capacitors (u-caps), have a symmetric input and output specific power. Their power density is ten times than that of a typical Lithium-ion battery and their energy density is four times than that of a typical double-layer capacitor [7, 8]. In addition, they offer higher cycle life, lower Equivalent Series Resistance (ESR) and reduced susceptibility to high depth-of-discharge.

The new LIC technology combines the intercalation mechanism of traditional Li-Ion batteries with the cathode of EDLCs, as shown in Fig. 2.4(a) [9]. The cathode employs activated carbon material at which charges are stored at the interface between the carbon and the electrolyte. The anode is generally pre-doped with Lithium ions, resulting in a lower anode voltage, and a higher cell voltage of 3.8-4 V versus 2.5-2.7 V for EDLCs [9]. As a consequence, same capacity LICs have 2-4× higher energy density than EDLCs, as shown in Fig. 2.4(b). LICs are well suited in the proposed battery cell cycler where relatively high energy (for power smoothing in time-scale of minutes) and high cycle-life (for long-time operation of the cell tester) are required. LICs with a nominal capacity of 3300 F and energy density of 12 Wh/kg are used in the system to handle the required energy. Two of these LICs are connected in series to provide the required voltage range by the system.

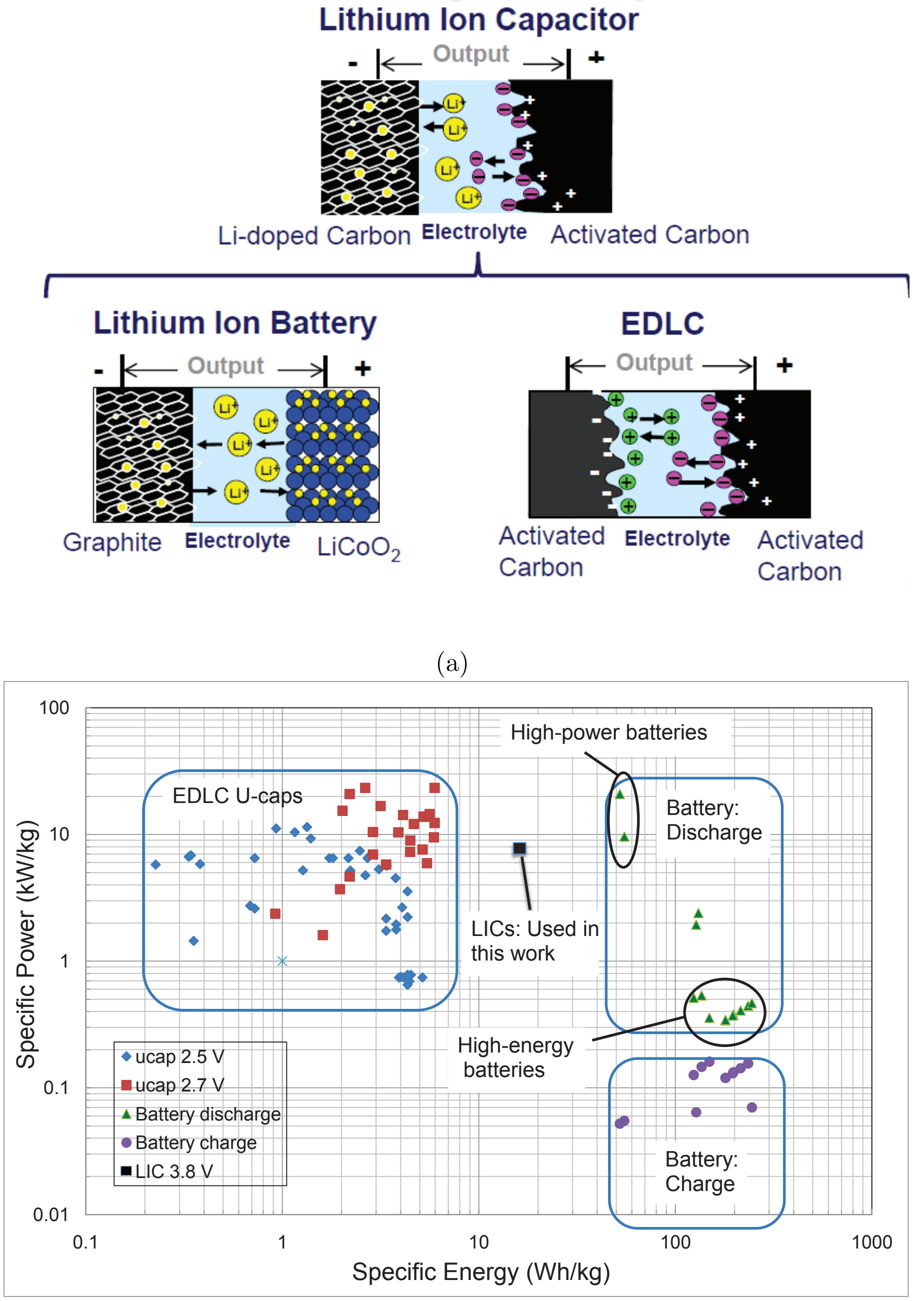

(a)

(b)

Figure 2.4: (a) Physical structure of Li-Ion Capacitor (courtesy of JSR Micro) [9]. (b) Ragone plot for different storage technologies [10].

3. **Inverter**

An off-the-shelf 250 W grid-tied single-phase inverter is used to transfer the battery power to the grid when the battery is discharging. The inverter is originally intended for micro wind turbine applications, where its power-voltage (P-V) profile can be programmed based on the turbine specifications. The P-V profile can be configured based on the slope of power versus voltage (S_{p-v}) and the cut-off voltage ($V_{inv,cut}$). The rated minimum and maximum operating input voltage of the inverter (V_{inv}) are 25 V and 50 V, respectively. For achieving higher efficiency and stability S_{p-v} and $V_{inv,cut}$ are designed to be 25 W/V and 25 V, respectively. The desired P-V profile along with some other examples are shown in Fig. 2.5.

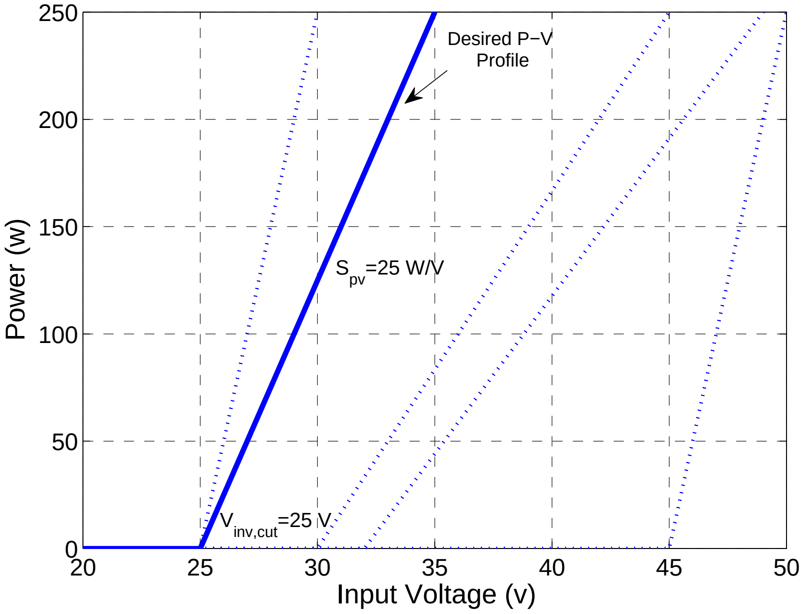

Figure 2.5: Inverter P-V profile.

2.2.1 Cycler Board Design

The cycler board with its novel architecture, which acts as an interface between the battery, inverter and the power supply, is made up of two dc-dc converters. The first dc-dc converter connects the battery to the LICs (main bus), and controls the battery current (I_{bt}). Due to the voltage range of the bus (5.7-7.6 V) and the battery (3-4.2 V), this converter is designed as a bi-directional synchronous buck converter. The second dc-dc converter connects the main bus to the inverter and controls the bus voltage (V_{uc}) keeping it within the safe range of operation. This converter is designed as a boost converter connecting the main bus (5.8-7.6 V) to the inverter (25-35 V).

The cycler board configuration is shown in Fig. 2.6(a) where the buck and boost converters have two interleaved phases. The use of a two-phase interleaved architecture offers lower output voltage ripple, and higher efficiency due to the lower conduction losses as compared to the non-interleaved architecture [11, 12]. Ideal inductor currents (i_L) and i_{bt} for the interleaved two-phase converter are shown in Fig. 2.6(b), where f_s is the switching frequency of the converter.

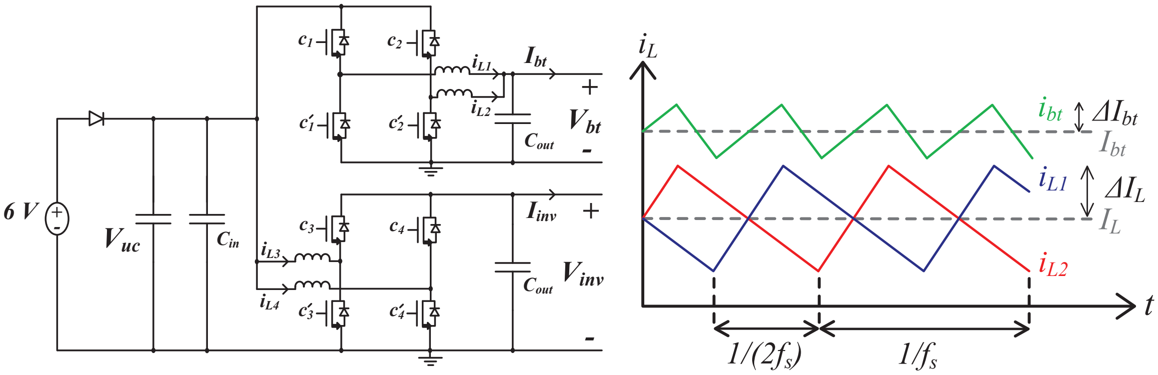

(a) (b)

Figure 2.6: (a) The cycler board configuration. (b) Ideal inductor current for an interleaved double-phase converter.

2.3 Controller Design

The digital controller of the multi-channel cell testing platform (shown in Fig. 2.7) requires two levels of control due to the existence of multiple channels. The central controller monitors the channels and sends the desired current references to the platform, while the local controller which is designed and implemented for each channel, controls the converters by sending PWM signals. The main purpose of the high-level controller is to send the battery current references to the channels based on the cycling plan. This controller monitors the voltage, current and temperature of the batteries to ensure the safe operation of the system, and logs these parameters for historical analysis. The main purpose of each local controller is to regulate the I_{bt} while the V_{uc} is maintained within the safe range. In addition, V_{inv} has to be maintained above 25 V to avoid the inverter from shutting down. This fail-safe mechanism increases the stability of the system. The local controller is made up of two sub-controllers which control the buck and the boost converters.

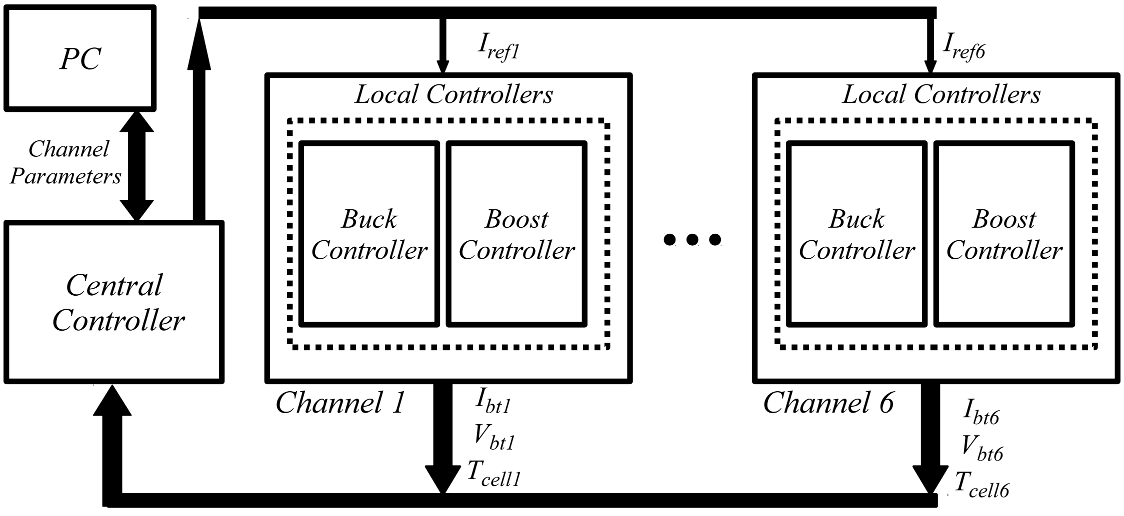

Figure 2.7: Controller diagram of the cell cycler.

The controller of the buck converter operates in Average Current Mode Control (ACMC) to regulate I_{bt} [13–16], while the controller of the boost converter operates in two voltage control modes. The operation modes of the boost controller are shown in Fig. 2.8. It should be noted that the minimum operating inverter voltage is 25 V, hence, if V_{inv} drops below 25 V, the inverter turns off. In the first mode, where $V_{uc} < 7$ V, the controller regulates the V_{inv} to 26 V to ensure the continued operation of the inverter. In the second mode, where $V_{uc} > 7$ V, the controller regulates V_{uc} to 7 V to ensure the safe operation voltage of the LICs. When $V_{uc} > 7$, the controller regulate V_{uc} by sending more power to the inverter.

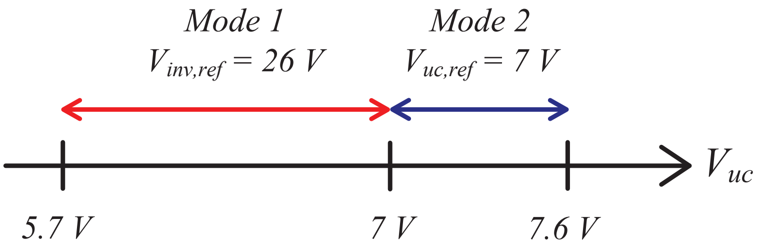

Figure 2.8: Operation modes of the boost converter controller.

The controller of the bi-directional buck converter is shown in Fig. 2.9(a) where a digital PI controller regulates the current of the phases by adjusting their duty cycles [17–20]. The controller of the boost converter in mode 1 and 2 are shown in Fig. 2.9(b) and (c), respectively. In mode 1, the boost controller operates in voltage-mode to regulate the converter output voltage (V_{inv}) to 26 V by adjusting the PWM signals. However, in mode 2, it operates in voltage-mode to regulate converter input voltage (V_{uc}). In order to regulate V_{uc}, the extra power is required to be transmitted to the inverter, therefore, inductor currents are adjusted to deliver this extra power to the inverter [21, 22].

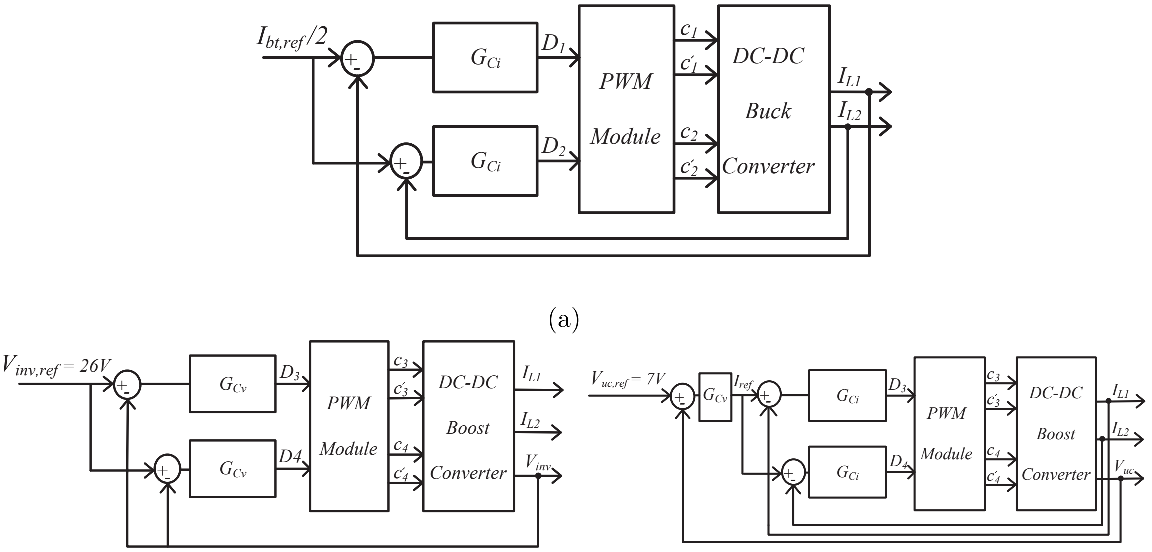

(a)

(b)

(c)

Figure 2.9: Control diagram of (a) the buck converter and the boost converter in (b) mode 1 and (c) mode 2.

To illustrates the cycler operation, a scenario is shown in Fig. 2.10. In the beginning, I_{bt} is zero and V_{uc} is 5.7 (diode on), therefore, the boost converter is in mode 1, regulating V_{inv} to 26 V (Fig. 2.11(a)). When I_{bt} is 20 A (Fig. 2.11(b)), V_{uc} increases but it is still lower than 5.8 V and therefore, the diode is still on. In the above time intervals, the power required by the inverter is supplied by the power supply.

The diode turns off when V_{uc} gets higher than 5.8 V (Fig. 2.11(c)), and the power required by the inverter is only supplied by the LICs. When V_{uc} gets higher than 7 V (Fig. 2.11(d)), the boost controller regulates the V_{uc} to 7 V (boost controller is in mode 2) by sending more power to the inverter. Therefore, the inverter voltage increases in order to sink the required amount of power. When I_{bt} gets negative (Fig. 2.11(e)) the battery starts charging and V_{uc} starts decreasing while the diode is still off. The diode turns on (Fig. 2.11(f)) when V_{uc} drops below 5.8 V.

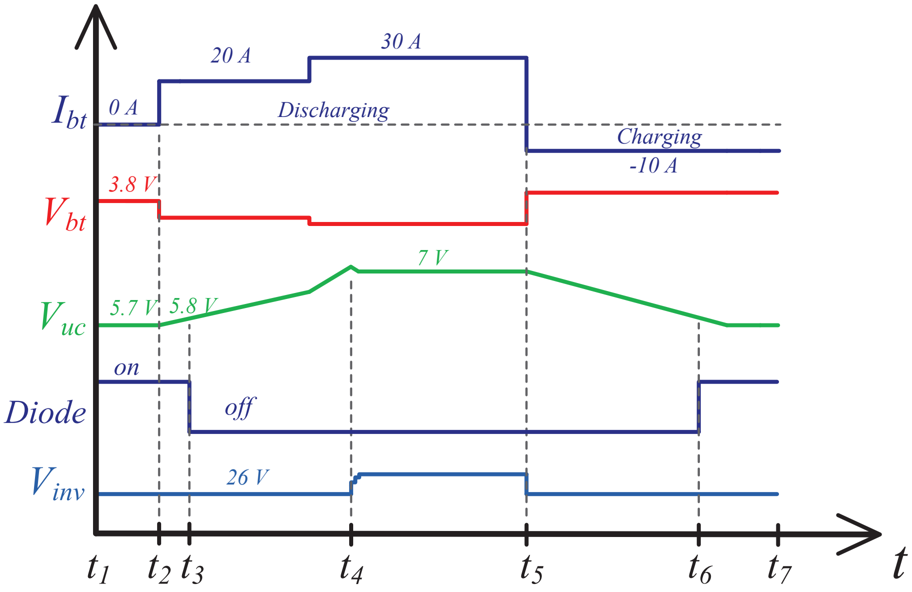

Figure 2.10: Operation diagram.

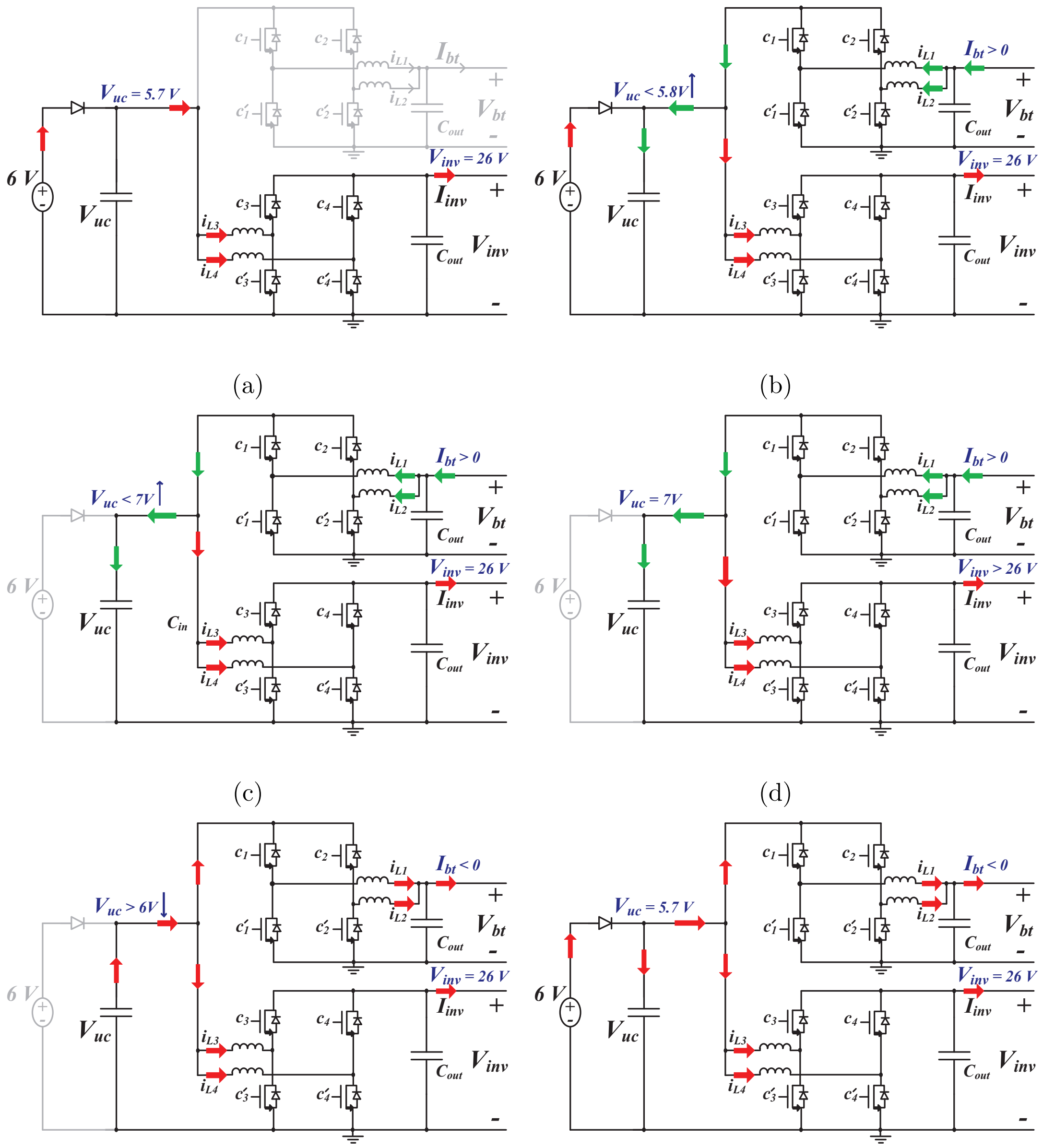

(a) (b)

(c) (d)

(e) (f)

Figure 2.11: Power flow in time intervals of (a) t_1-t_2, (b) t_2-t_3, (c) t_3-t_4, (d) t_4-t_5, (e) t_5-t_6 and (f) t_6-t_7.

2.4 System Implementation and Results

The implemented cell cycler system with the cycler board and off-the-shelf components is shown in Fig. 2.12(a). The designed 300 W (the maximum deliverable power by the battery is 296 W (80 A - 3.7 V)) cycler board, which consists of two-phase converters is shown in Fig. 2.12(b). Two individual microcontrollers (dsPIC30F2020) are used to control the converters. The specifications of the converters are listed in Table 2.3.

Table 2.3: Experimental System Parameters

Buck Converter (Each Phase)	Value	Unit
U-Cap Voltage, V_{uc}	4.6-7.6	V
Battery Voltage, V_{bt}	3-4.2	V
Switching Frequency, f_s	200	kHz
Max. Power, P_{max}	150	W
Inductors, L	3.3	μH
Inductor ESR, R_L	1.5	mΩ
Saturation Current, $I_{L,sat}$	48	A
MOSFET on-resistance, R_{on}	1.7	mΩ
Boost Converter (Each Phase)		
U-Cap Voltage, V_{uc}	4.6-7.6	V
Max. Inverter Voltage, V_{inv}	35	V
Switching Frequency, f_s	200	kHz
Max. Power, P_{max}	150	W
Inductors, L	10	μH
Inductor ESR, R_L	2.6	mΩ
Saturation Current, $I_{L,sat}$	18	A
MOSFET on-resistance, R_{on}	3.2	mΩ

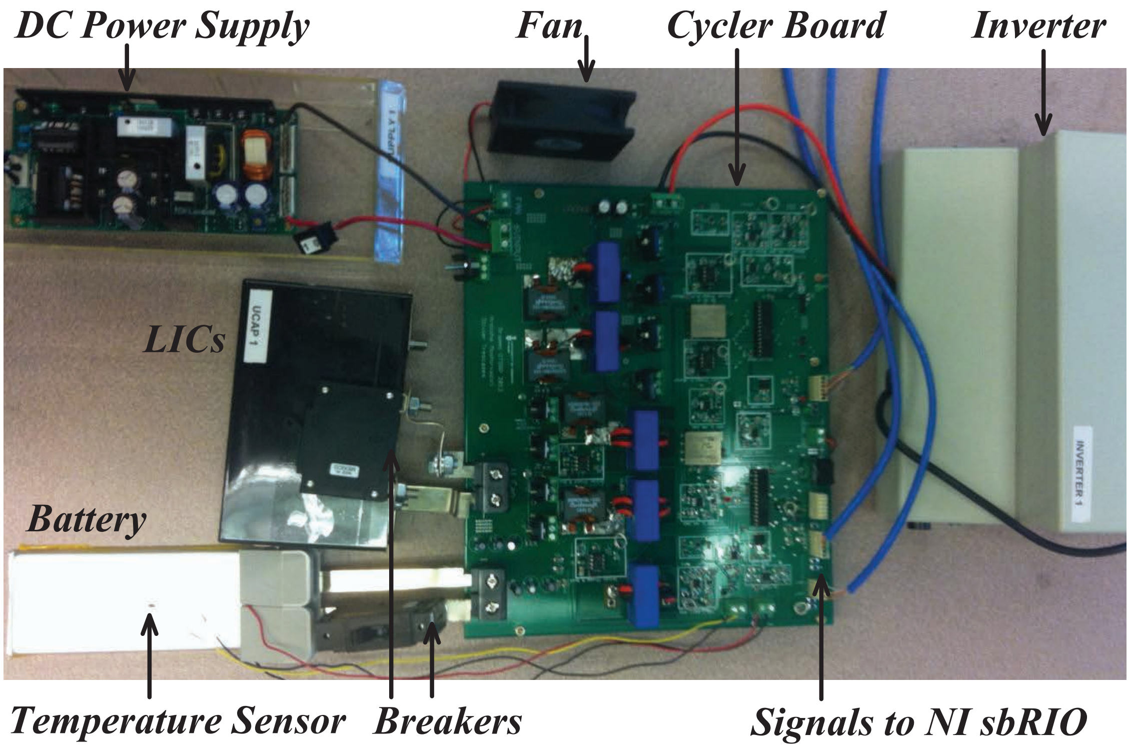

(a)

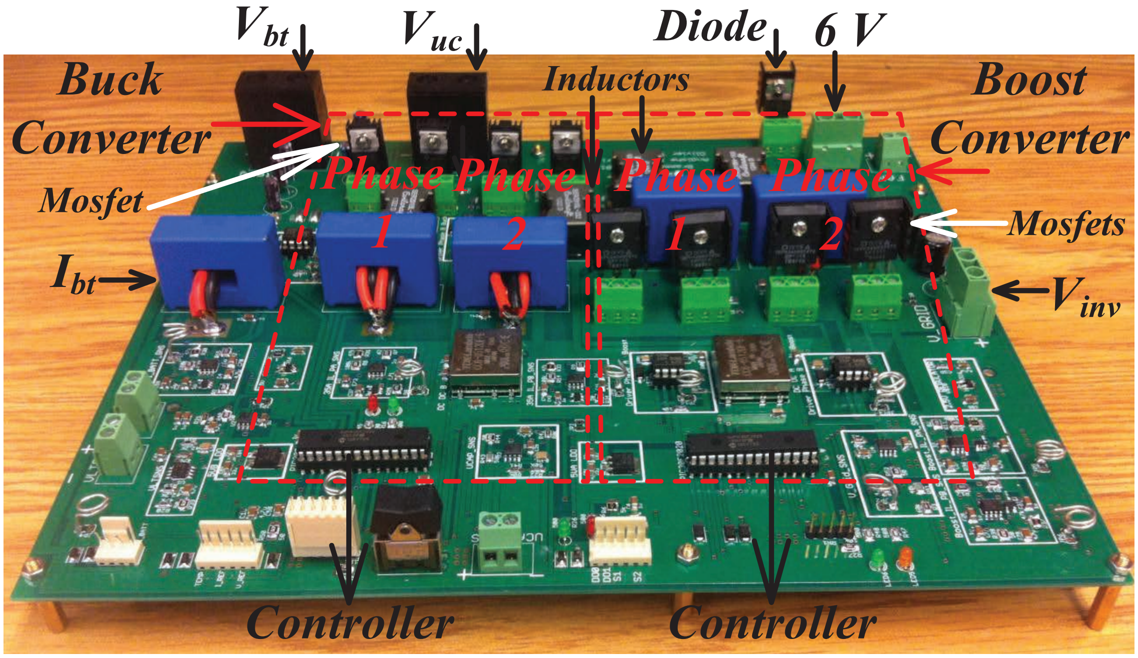

(b)

Figure 2.12: Implementation of the (a) cell cycler and (b) cycler board.

The operation of the buck converter in steady state is illustrated in Fig. 2.13(a), where the switching frequency is 200 kHz (to achieve high efficiency). The average value and the peak-to-peak ripple of interleaved inductor currents (i_{L1}, i_{L2}) are 15 A and 2 A, respectively. The response of the buck converter to a 40 A step (10 A/div) in battery reference current is shown in Fig. 2.13(b). The settling time (10%-90%) of the response is less than 5 ms, while the response overshoot is less than 5%. The steady state operation of the boost converter in mode 1 (regulating V_{inv} to 26 V) is shown in Fig. 2.13(c), where the converter is switching at 200 kHz.

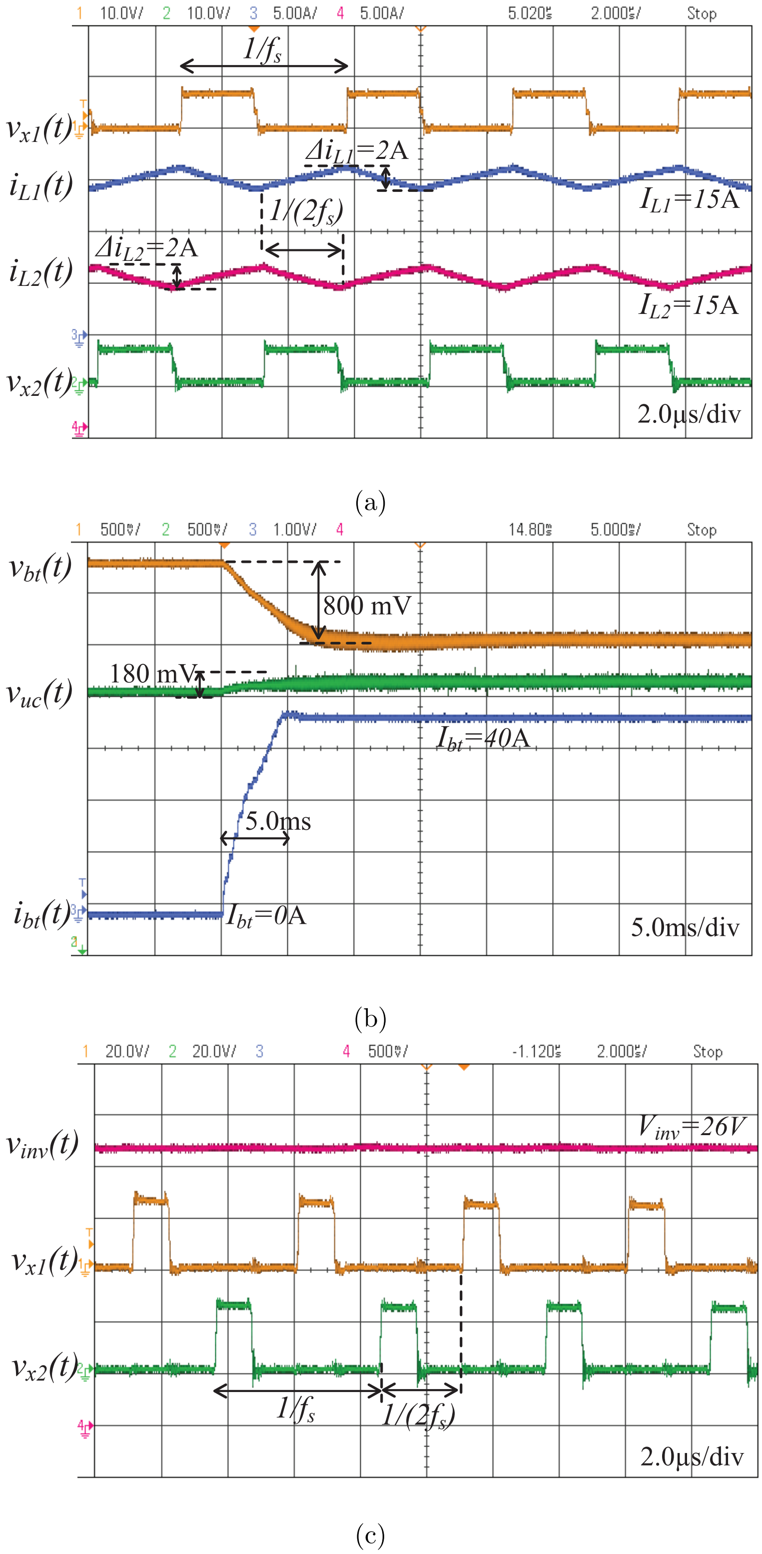

Figure 2.13: (a) Steady state and (b) current step response of the buck converter. (c) Steady state response of the boost converter.

The current profile scenario discussed in 2.3, is experimentally tested on the cycler system, and the results are shown in Fig. 2.14. In the beginning, I_{bt} is zero and V_{inv} is regulated to 26 V (boost converter is in mode 1). When V_{uc} gets higher than 7 V, the boost controller regulates V_{uc} to 7 V (boost controller is in mode 2) by sending the more power to the inverter. Therefore, the inverter voltage increases in order to sink the required amount of power. When I_{bt} gets negative, and battery starts charging, V_{uc} starts decreasing and V_{uc} is regulated to 26 V.

It should be noted that the cycler is designed for 300 W - 80 A , however, the continuous discharge power of the battery is lower than 200 W (the maximum discharge current of the battery is 50A). The measured efficiency of the cell cycler for the input power of 160 W (4 V, 40 A) is 82.5%.

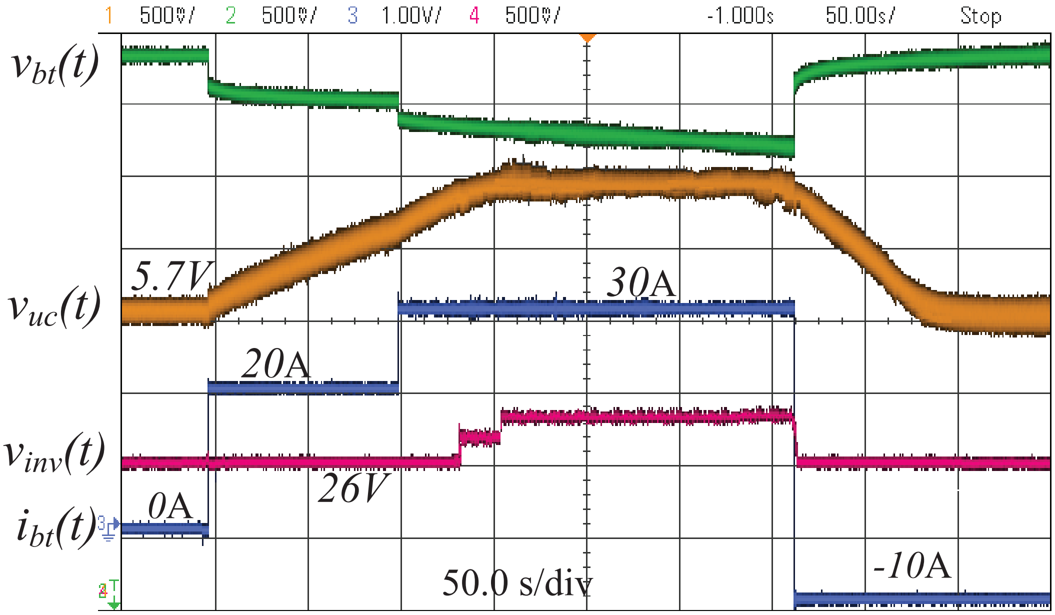

(a)

Figure 2.14: Experimental V_{bt}, V_{uc} and V_{inv} during the system operation under the sample current profile.

The regenerative six-channel cell testing platform is implemented as shown in Fig. 2.15(a). The six channels operate in parallel and are individually programmed based on the specific cycling plan as shown in Table 2.2. An NI single-board RIO (sbRIO) FPGA platform is utilized as the main controller to send the desired current profiles to the channels. The sbRIO is controlled in real-time by a designed LabVIEW program. The front panel of the LabVIEW program is shown in Fig 2.15(b), where the user can control the channels and set the safety limits.

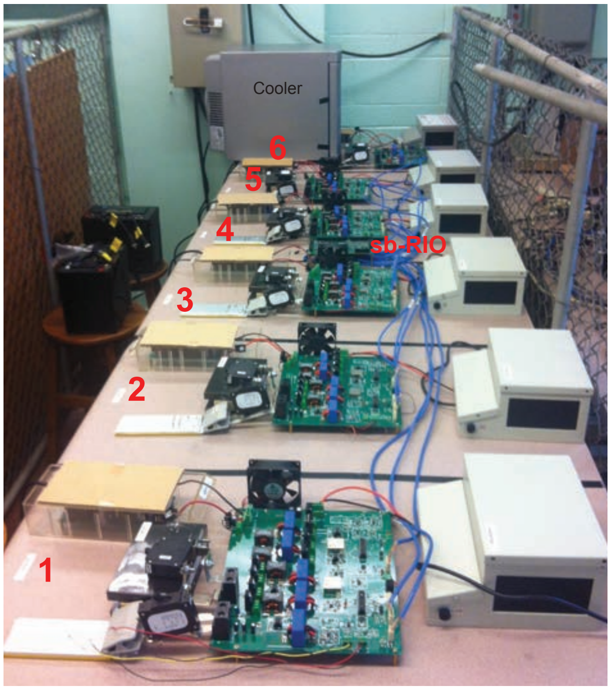

(a)

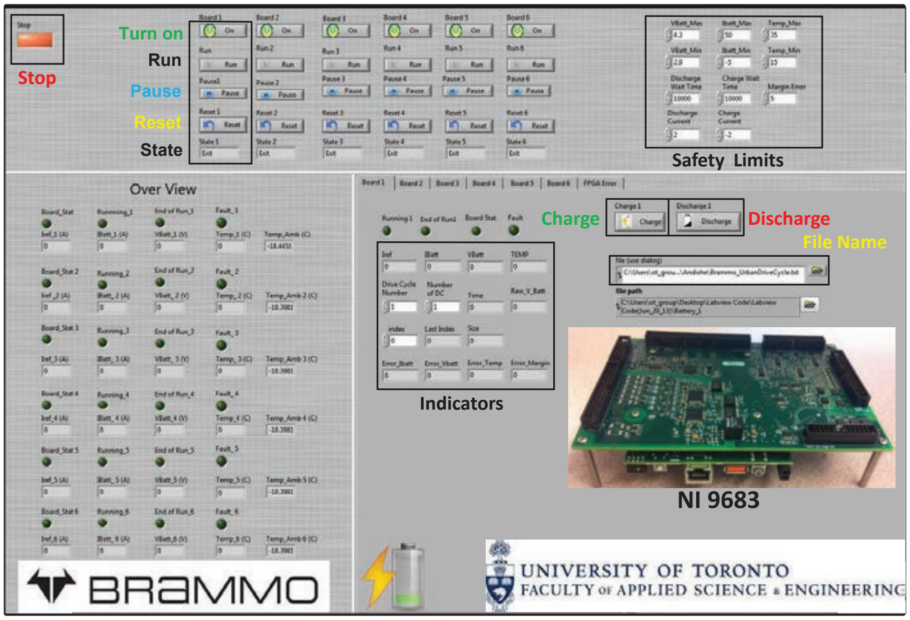

(b)

Figure 2.15: (a) Six channel cell testing platform. (b) Front panel of the LabVIEW program.

2.5 Chapter Summary and Conclusion

In this Chapter, a regenerative multi-channel cell testing platform is proposed. This platform is designed for investigating the long-term effects of temperature, average current and dynamics of the current profile of EVs on lifetime of Li-Ion batteries. Industrial cell testers are not ideal for this application as they usually lack one or more of the following properties: regenerative ability and high current bandwidth. The novel architecture of the proposed cell cycler utilizes a grid-tie single phase inverter for each channel and LICs to overcome the above mentioned challenges. In addition, the cycler system is programmable, meaning that the users can program their desired current commands to be sent to the system. The battery cell cycler is designed to be modular to enable the addition of more channels by utilizing off-the-shelf components. The 300 W and 5 V cycler system is designed and implemented. The experimental results of the cycler prove the stable closed-loop operation of the system. The cycler system has the ability to follow the current dynamics of up to 8 A/ms.

References

[1] Brammo, Inc. Accessed in August 2013, available at http://www.brammo.com/home/.

[2] Gaus sts power electronics. Accessed in August 2013, available at http://www.gaus-sts.com/index.html.

[3] C8000 Battery Testing System, CADEX. Accessed in August 2013, available at http://www.cadex.com/products/c8000-battery-testing-system.

[4] T. F. Wu, K. H. Sun, C. L. Kuo, M.-S. Yang, and R.-C. Chang, "Design and implementation of a 5 kw bi-directional inverter with wide inductance variation," in *Energy Conversion Congress and Exposition (ECCE), 2010 IEEE*, pp. 45–52, 2010.

[5] T. F. Wu, C. H. Chang, H.-C. Wu, J.-R. Ciou, and T.-S. Lin, "Predictive digital controlled three phase bi-directional inverter with wide inductance variation," in *Energy Conversion Congress and Exposition (ECCE), 2010 IEEE*, pp. 37–44, 2010.

[6] D. Thrimawithana, U. Madawala, and Y. Shi, "Design of a bi-directional inverter for a wireless v2g system," in *Sustainable Energy Technologies (ICSET), 2010 IEEE International Conference on*, pp. 1–5, 2010.

[7] "48 V ultracapacitor specifications." Maxwell Technologies Inc. datasheet, 2011. available at http://maxwell.interconnectnet.com/.

[8] "U-charge xp lithium iron magnesium phospate battery." Valence Technology datasheet, 2010. Available at http://www.valence.com/energy-storage/xp-12v-19v-lithium-phosphate-battery-module.

[9] "Lithium Ion Capacitor." JSR Micro, 2012. Available at http://www.jsrmicro.com/index.php/EnergyAndEnvironment/LithiumIonCapacitor/.

[10] O. Laldin, M. Moshirvaziri, and O. Trescases, "Predictive algorithm for optimizing power flow in hybrid ultracapacitor/battery storage systems for light electric vehicles," *IEEE Transactions on Power Electronics*, vol. 28, no. 8, pp. 3882–3895, 2013.

[11] H. B. Shin, J. G. Park, S. K. Chung, H. W. Lee, and T. Lipo, "Generalised steady-state analysis of multiphase interleaved boost converter with coupled inductors," *Electric Power Applications, IEE Proceedings* -, vol. 152, no. 3, pp. 584–594, 2005.

[12] R.-L. Lin, C.-C. Hsu, and S.-K. Changchien, "Interleaved four-phase buck-based current source with center-tapped energy-recovery scheme for electrical discharge machining," *Power Electronics, IEEE Transactions on*, vol. 26, no. 1, pp. 110–118, 2011.

[13] R. Li, "Modeling average-current-mode-controlled multi-phase buck converters," in *Power Electronics Specialists Conference, 2008. PESC 2008. IEEE*, pp. 3299–3305, 2008.

[14] J. Morales, J. Leyva-Ramos, E. Carbajal, and M. Ortiz-Lopez, "Average current-mode control scheme for a quadratic buck converter with a single switch," *Power Electronics, IEEE Transactions on*, vol. 23, no. 1, pp. 485–490, 2008.

[15] S. Kancherla and R. Tripathi, "Nonlinear average current mode control for a dc-dc buck converter," in *Sustainable Energy Technologies, 2008. ICSET 2008. IEEE International Conference on*, pp. 831–836, 2008.

[16] J.-J. Chen, B.-H. Hwang, C.-M. Kung, W.-Y. Tai, and Y.-S. Hwang, "A new single-inductor quadratic buck converter using average-current-mode control without slope-compensation," in *Industrial Electronics and Applications (ICIEA), 2010 the 5th IEEE Conference on*, pp. 1082–1087, 2010.

[17] P. Gayathiridevi, S. Vijayalakshmi, and K. Vairamani, "Discrete controller for high frequency buck converter," in *Circuits, Power and Computing Technologies (ICCPCT), 2013 International Conference on*, pp. 605–610, 2013.

[18] S. Mitra, L. H. Keel, and S. Bhattacharyya, "Data based design of digital pid controller," in *American Control Conference, 2007. ACC '07*, pp. 226–230, 2007.

[19] L.-S. Su, "Digital controller - its design techniques," in *Instrumentation and Measurement Technology Conference, 1994. IMTC/94. Conference Proceedings. 10th Anniversary. Advanced Technologies in I amp; M., 1994 IEEE*, pp. 841–844 vol.2, 1994.

[20] H. Seraji, "Design of discrete pid controllers for pole placement," in *Decision and Control, 1984. The 23rd IEEE Conference on*, vol. 23, pp. 1721–1722, 1984.

[21] C.-H. Hsu, T.-W. Chang, and C.-L. Wey, "A voltage-mode hysteretic boost dc-dc converter with dual control modes," in *Microelectronics and Electronics (PrimeAsia), 2012 Asia Pacific Conference on Postgraduate Research in*, pp. 67–71, 2012.

[22] C. Yao, X. Ruan, W. Cao, and P. Chen, "A two-mode control scheme with input voltage feed-forward for two-switch buck-boost dc/dc converter," 2013.

Chapter 3

Battery Modeling

3.1 Introduction

In this chapter, a novel approach is proposed to design a dynamic electrical battery model for use in real-time BMS, as described in Section 1.2. The novelty within this approach is that the model parameters are dynamically updated based on SOC and cell temperature. Modeling of a commercially available Li-Ion battery using the proposed approach is presented, and the model is experimentally validated.

Battery modeling plays a significant role in EV technologies. Battery models are utilized by EV designers to optimally size the required ESS of an EV and to predict the performance of the ESS. In addition, battery models are used as a powerful tool for on-line self-learning performance and SOC estimation in BMS [1–6]. As EVs today use Li-Ion batteries due to their high energy density [7, 8], accurate Li-Ion battery models are required. It is critical for the battery models to consider thermal behavior of the battery for lifetime and safety considerations [2, 9]. Various battery models for different applications have been developed. Electrochemical models are used to optimize the physical aspects of batteries and characterize power, voltage and current parameters [10, 11]. Mathematical models [12, 13] are useful to designers for estimating battery runtime, efficiency, or capacity using mathematical methods like stochastic approaches [1]. However, electrochemical and mathematical models are not suitable for real-time BMS targeted application. Electrical models utilize equivalent circuit components to predict the terminal characteristics of the batteries (their current and voltage). Also, electrical battery models enable a systematic design approach for electric vehicles.

There exist several approaches in the literature for modeling batteries in the electrical domain. In [1], an Li-Ion battery model capable of predicting runtime and I-V performances of the battery is proposed. However, temperature variation is not taken into account in their calculation. In [2, 14], dynamic models are proposed for Li-Ion batteries which consider the cell temperature. However, these models do not dynamically update the model parameters based on cell temperature variations due to self heating. In the following sections, the proposed battery modeling approach is discussed, a modeling example is provided.

3.2 Electrical Battery Modeling

A common electrical and empirical battery model is shown in Fig. 3.1 [15–18]. This model consists of three components: an open circuit voltage, V_{OC}, a series resistance, R_0, and a cascade of RC circuits. The internal equivalent inductance of the battery which represents the inductance of the connectors is ignored due to its negligible effect. V_{OC} represents the steady state terminal voltage of the battery under the open-circuit condition and is a monotonic function of the SOC. R_0 represents the electrical resistance between the terminal contacts and the electrodes. The cascade of RC circuits arise from two phenomena. The voltage drops on the resistors represent the required polarization potential to activate the electrochemical reaction of the battery [15]. The capacitors represent the structure of the battery and characterize the transient response of the electrodes [15,16]. V_{OC} is SOC dependent, and it has a minor dependency on temperature and SOC [17]. R_0 is a function of temperature and the RC circuits are functions of temperature and SOC [16, 17].

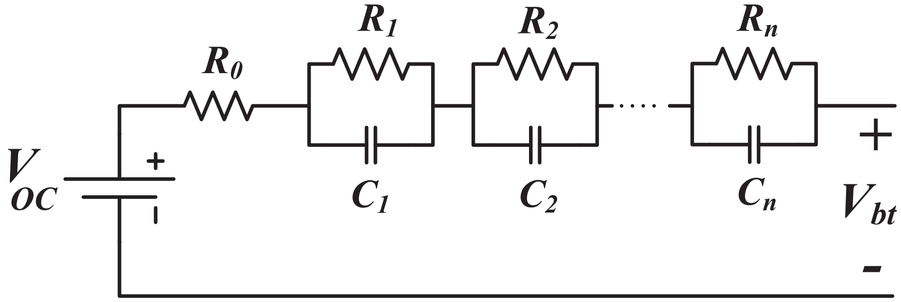

Figure 3.1: Common electrical battery model.

3.2.1 Proposed Modeling Approach

In the proposed battery modeling approach, the model parameters are dynamically updated based on cell temperature and SOC variations. Therefore, the dynamic battery behaviour may be more accurately predicted. This is because the battery impedance is inversely proportional to its temperature. Hence, if self heating is not taken into consideration, under estimation could be made with regards to the battery capability, as self-heating directly increases the cell temperature enabling the battery to operation more.

The effect of SOC variation is only taken into account to update the V_{OC} parameter. The RC circuits parameters are not updated due to SOC variations as these parameters are minimally affected at frequencies of interest for EVs.

A battery model based on this approach is described below:

1. The effect of SOC on the V_{OC} parameter may be obtained by discharging the battery with nominal discharge current based on a given SOC interval step. Upon applying each step, the battery is given time to rest until steady state is reached, and afterwards V_{OC} is measured.

2. The internal impedance of the battery is measured at various temperatures conditions. The battery internal impedance (Z) is obtained through sinusoidally perturbing the frequency of the discharge current while measuring the battery voltage.

3. Curve fitting methods are applied to obtain the resistive and capacitive component values based on the measured internal impedance at the various temperature conditions.

4. Based on the collected data, the model parameters are dynamically updated based on self heating. A thermal model is utilized to obtain the cell temperature based on the operating condition of the cell.

It should be noted that the battery model used in this approach is a small-signal model, therefore, the model has limitations on current swings.

3.3 Modeling Example

In this section, the model for the Li-Ion battery discussed in Chapter 2, is derived utilizing the proposed modeling approach.

3.3.1 V_{OC} Parameter Determination

The obtained V_{OC} versus SOC of the battery is shown in Fig. 3.2. The battery was discharged with the nominal discharge current of 10 A.

3.3.2 Internal Impedance Measurements

The test setup for impedance measurement is shown in Fig. 3.3. The electrical load is used to provide the current perturbation. The programmable function generator is used as an interface to provide the sinusoidal reference current profile to the load. The battery voltage and current are sampled by the oscilloscope and transmitted to the computer for

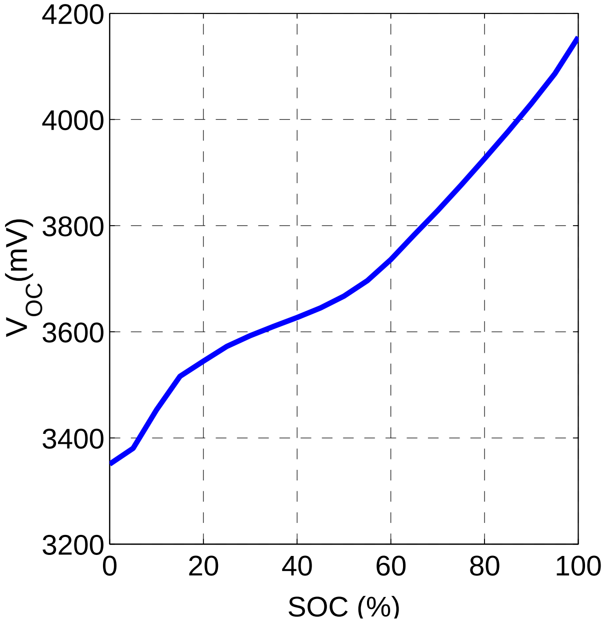

Figure 3.2: V_{OC} versus SOC curve.

digital post processing. The cooler (a chamber to maintain the temperature) was used to regulate the battery temperature.

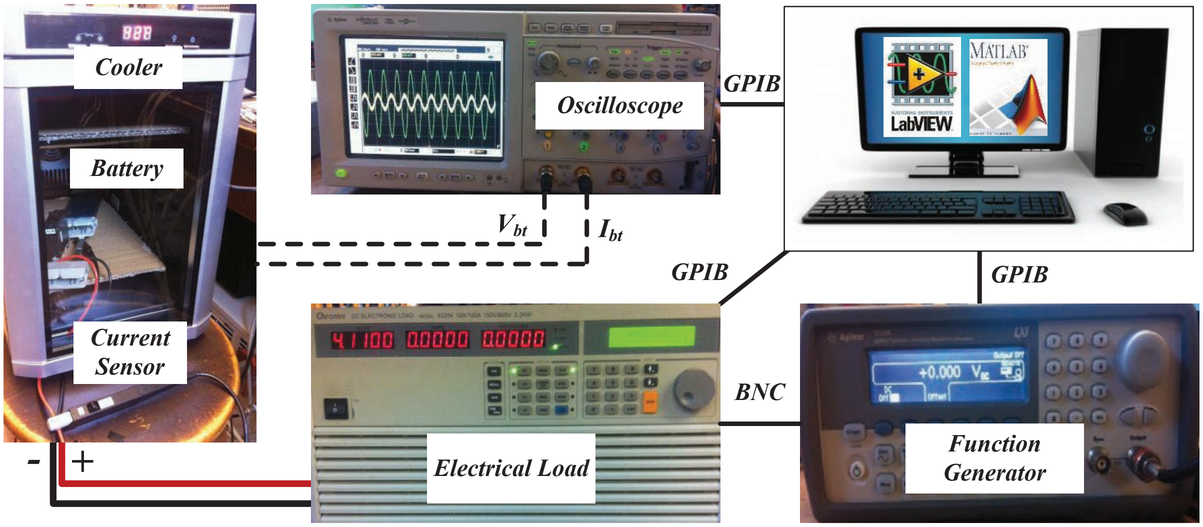

Figure 3.3: Impedance measurement setup.

The Nyquist plot for the measured impedance measurements is shown in Fig. 3.4.

The battery impedance can be defined as follows:

$$Z \quad = \quad Re[Z] + jIm[Z] \tag{3.1}$$

where $Re[Z]$ and $Im[Z]$ are the real and imaginary parts of the impedance, respectively. The impedance is measured within a temperature range of 5°C to 20°C and a frequency range of 0.07 Hz to 7 kHz (based on the bandwidth limitation of the equipment). For frequencies higher than 1 kHz, the imaginary part of the impedance is positive, which shows the inductive behaviour of the terminal connectors of the battery.

From Fig. 3.4, the motivation behind considering the self heating effect to dynamically update the model parameters is further justified. For example, the internal resistance of the battery is almost halved from 5°C to 20°C at low frequencies.

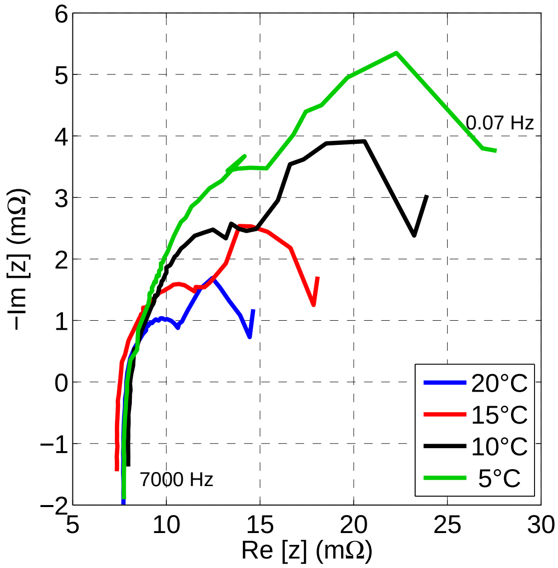

Figure 3.4: Measured Nyquist curve for cell impendence.

3.3.3 Resistive and Capacitive Parameter Extraction

Using the obtained impedance plots, the resistive and capacitive parameters are extracted through the curve fitting method (least square error [19]). It was found that for the current profile of interest, which is the urban drive-cycle mentioned in Chapter 2, sufficient model accuracy is obtained with a third order model which considers R_0 and three RC circuit stages. The accuracy improvement from a third order model to a fifth order model is only in the order of 1%. This is also apparent in Fig. 3.5(a) where the simulated battery voltage in response to the urban drive-cycle profile (shown in Fig. 3.5(b)) are plotted for up to fifth order battery models. Therefore, for the real-time application in the BMS systems, a third order model is selected.

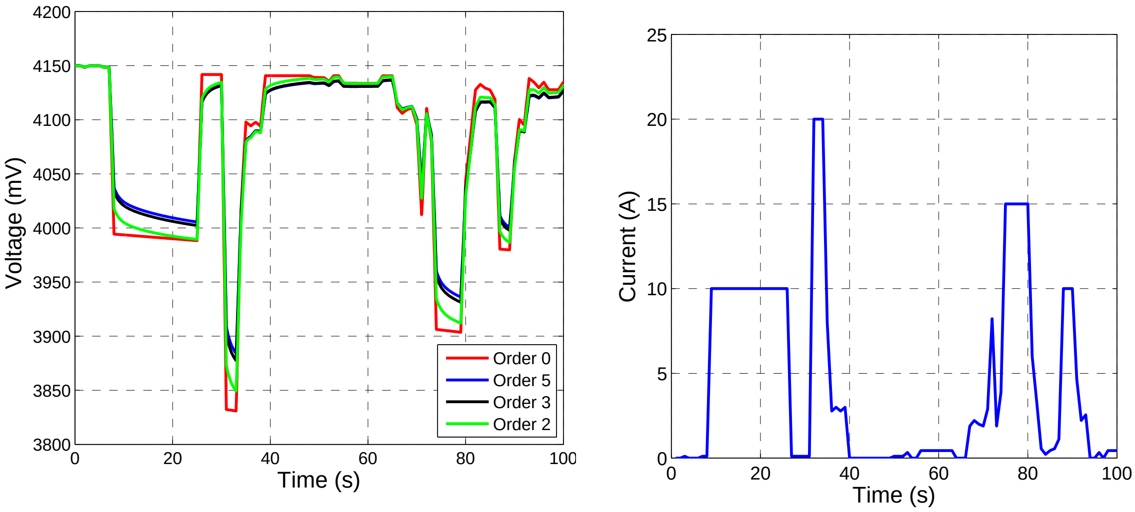

(a) (b)

Figure 3.5: Simulated (a) V_{bt} for different orders and (b) simulated I_{bt}.

The impedance of the third order model is as follows:

$$Z = R_0 + (R_1 \| \frac{1}{j2\pi f C_1}) + (R_2 \| \frac{1}{j2\pi f C_2}) + (R_3 \| \frac{1}{j2\pi f C_3}). \tag{3.2}$$

The resistive and capacitive values are calculated utilizing the least square error curve fitting method [19] such that the above equation matches the measured battery impedance shown in Fig. 3.4. The list of resistive and capacitive values at four different temperatures are provided in Table. 3.1. As the impedance of the battery is measured at four different temperatures (see Fig. 3.6), the resistive and capacitive values are extracted at these temperatures. However, these parameters are extrapolated at lower and higher temperatures that are beyond the range of the thermal chamber.

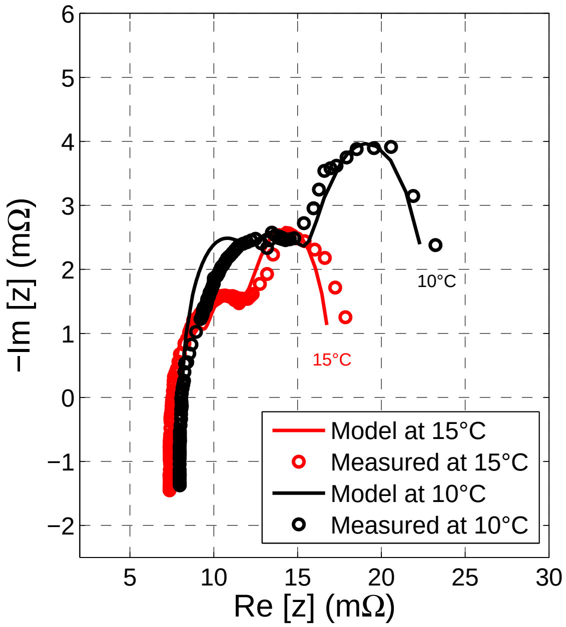

Figure 3.6: Simulated and experimental Nyquist curves for the cell impendence.

Table 3.1: Extracted Model Parameters

Parameter	Temperature (°c)				Unit
	5	10	15	20	
R_0	8.0	8.1	7.5	7.6	mΩ
R_1	4.3	4.1	1.9	1.0	mΩ
R_2	5.5	3.5	2.5	1.8	mΩ
R_3	10.0	7.5	5.1	3.2	mΩ
c_1	0.4	0.4	0.3	0.3	F
c_2	4.3	4.1	4.1	4.0	F
c_3	49.8	35.3	34.9	35.1	F

3.3.4 Dynamic Update of Model Parameters

To dynamically update the model parameters a thermal battery model is required. The thermal model predicts the cell temperature based on the its internal losses. The thermal model can be expressed by (3.3),

$$mC_p\frac{dT_{Cell}}{dt} = \sum_{i=0}^{3}\frac{V_i^2}{R_i} - h_{Conv}S_{Cell}(T_{Cell} - T_{Ambient}), \tag{3.3}$$

where m is the battery mass (kg), C_p is the specific heat (J/kgK), V_i is the voltage drop on R_i, h_{Conv} is the heat transfer coefficient (W/m^{2}K) and S_{Cell} is the cell surface area [20]. Having obtained the battery thermal model, the electrical model parameters can now be dynamically updated as illustrated in Fig. 3.7.

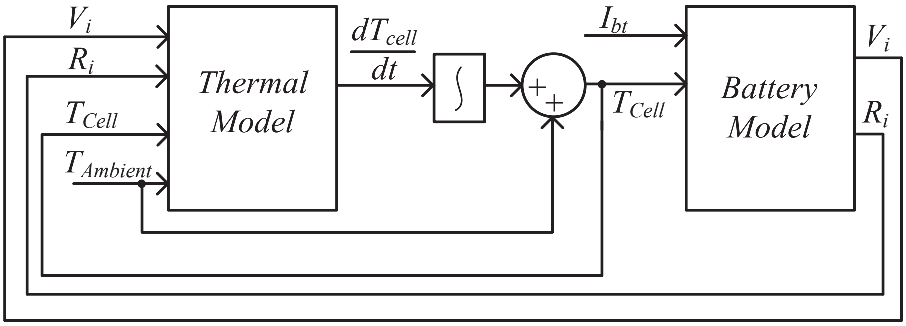

Figure 3.7: Block diagram showing the update process of the model parameters.

3.4 Model Validation

To validate the proposed modeling approach, the battery discharge curve and the battery behaviour under the urban drive-cycle are simulated and experimentally verified. The cycler system discussed in Chapter 2 was utilized to perform the experimental tests.

The simulated and experimental results of the battery voltage with respect to DOD at the discharge current of 2 C (20 A) at the room temperature (23°C) is shown in Fig. 3.8. The battery is discharged from the maximum voltage (4.2 V) to the cut-off voltage (3 V). The battery temperature increased by 10 °C, and the thermal model error is less than 3%.

The voltage response of the battery and the model to the urban drive-cycle at the room temperature (23°C)is shown in Fig. 3.9(a). The current profile of the battery is also shown in Fig. 3.9(b).

The maximum error of the battery voltage is less than 3.5%. It should be noted that maximum error of the experimental current is 4.7% and it is not considered in the error calculation of the model.

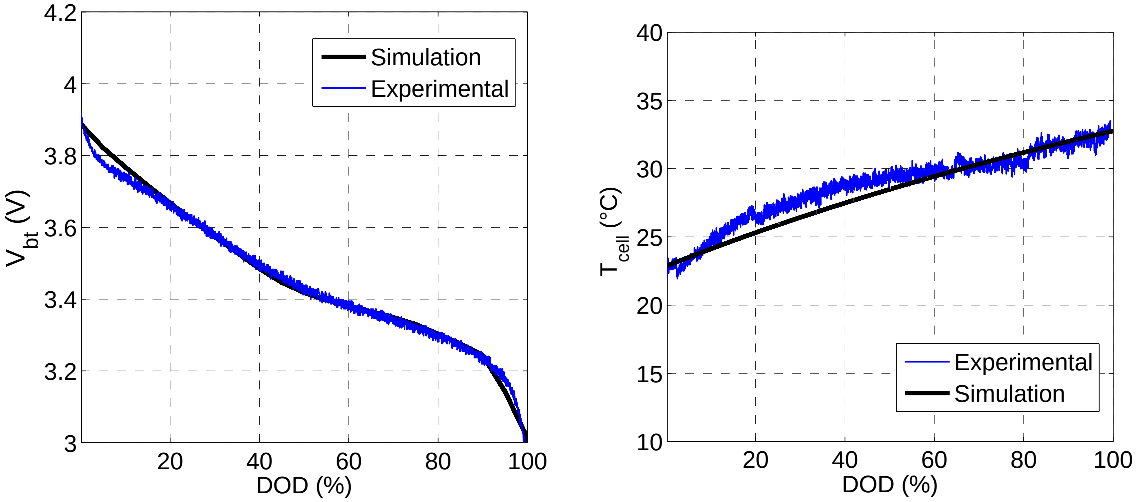

(a) (b)

Figure 3.8: Simulated and experimental (a) V_{bt} and (b) T_{Cell} for constant discharge current 2C (20 A).

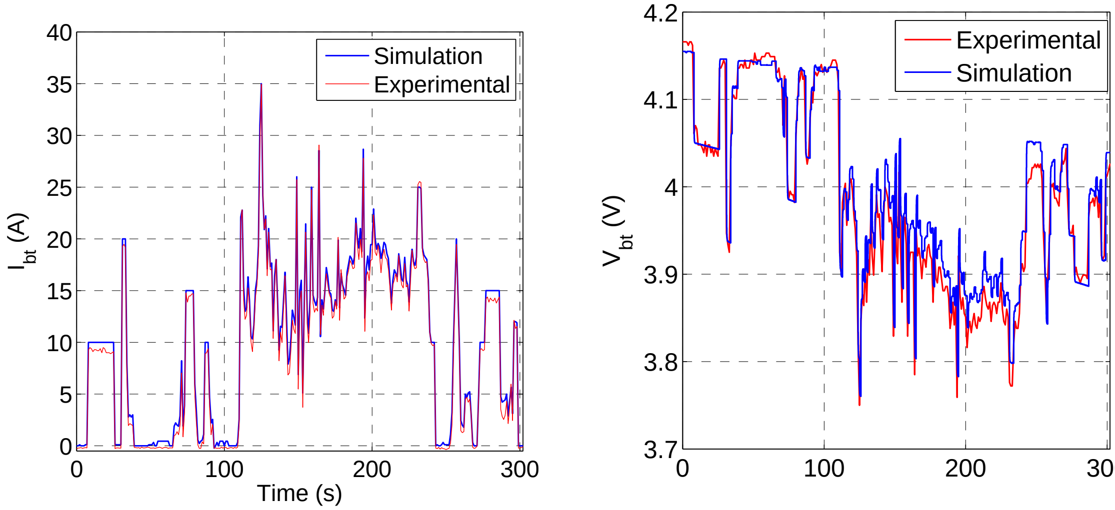

(a) (b)

Figure 3.9: Simulated and experimental (a) I_{bt} and (b) V_b for the urban drive-cycle.

3.5 Chapter Summary and Conclusion

In this chapter, an electrical battery modelling approach is proposed, where the model parameters are dynamically updated based on cell temperature and SOC variations. A modelling example of a commercialized Li-Ion battery is presented. The model parameters are extracted based on impedance and thermal measurements.

The accuracy of the model is verified by comparing the the simulation and experimental results under a constant and the urban drive-cycle current profiles. It is shown that the battery temperature rises by 11°C under 2 C discharge current at room temperature, and as a result the internal impedance decreases. Therefore, the benefit of adding self heating process to the model is further justified. Further improvement in the accuracy of the model, by updating the model parameters based on the effect of degradation, is considered for future work.

References

[1] M. Chen and G. Rincon-Mora, “Accurate electrical battery model capable of predicting runtime and i-v performance,” *Energy Conversion, IEEE Transactions on*, pp. 504–511, 2006.

[2] O. Erdinc, B. Vural, and M. Uzunoglu, “A dynamic lithium-ion battery model considering the effects of temperature and capacity fading,” in *Clean Electrical Power, 2009 International Conference on*, pp. 383–386, 2009.

[3] L. Lam, P. Bauer, and E. Kelder, “A practical circuit-based model for li-ion battery cells in electric vehicle applications,” in *Telecommunications Energy Conference (INTELEC), 2011 IEEE 33rd International*, pp. 1–9, 2011.

[4] J. Yan, C. Li, G. Xu, and Y. Xu, “A novel on-line self-learning state-of-charge estimation of battery management system for hybrid electric vehicle,” in *Intelligent Vehicles Symposium, 2009 IEEE*, pp. 1161–1166, 2009.

[5] A. Ostadi, M. Kazerani, and S.-K. Chen, “Optimal sizing of the energy storage system (ess) in a battery-electric vehicle,” in *Transportation Electrification Conference and Expo (ITEC), 2013 IEEE*, pp. 1–6, 2013.

[6] R. Balch, A. Burke, and A. Frank, “The affect of battery pack technology and size choices on hybrid electric vehicle performance and fuel economy,” in *Applications and Advances, 2001. The Sixteenth Annual Battery Conference on*, pp. 31–36, 2001.

[7] L. Mandal and R. Cox, “A transient-based approach for estimating the electrical parameters of a lithium-ion battery model,” in *Energy Conversion Congress and Exposition (ECCE), 2011 IEEE*, pp. 2635–2640, 2011.

[8] R. Spotnitz, “Advanced ev and hev batteries,” in *Vehicle Power and Propulsion, 2005 IEEE Conference*, pp. 4 pp.–, 2005.

[9] C. Mi, B. Li, D. Buck, and N. Ota, “Advanced electro-thermal modeling of lithium-ion battery system for hybrid electric vehicle applications,” in *Vehicle Power and Propulsion Conference, 2007. VPPC 2007. IEEE*, pp. 107–111, 2007.

[10] P. M. Gomadam, J. W. Weidner, R. A. Dougal, and R. E. White, “Mathematical modeling of lithium-ion and nickel battery systems,” *Journal of Power Sources*, vol. 110, no. 2, pp. 267 – 284, 2002.

[11] L. Song and J. W. Evans, “Electrochemical-thermal model of lithium polymer batteries,” *Journal of The Electrochemical Society*, vol. 147, no. 6, pp. 2086–2095, 2000.

[12] R. Rynkiewicz, “Discharge and charge modeling of lead acid batteries,” in *Applied Power Electronics Conference and Exposition, 1999. APEC ’99. Fourteenth Annual*, vol. 2, pp. 707–710, 1999.

[13] P. Pascoe and A. Anbuky, “Vrla battery discharge reserve time estimation,” *Power Electronics, IEEE Transactions on*, vol. 19, no. 6, pp. 1515–1522, 2004.

[14] J. Shen, S. Dusmez, and A. Khaligh, “An advanced electro-thermal cycle-lifetime estimation model for lifepo4 batteries,” in *Transportation Electrification Conference and Expo (ITEC), 2013 IEEE*, pp. 1–6, 2013.

[15] W. Luo, C. Lv, L. Wang, and C. Liu, “Study on impedance model of li-ion battery,” in *Industrial Electronics and Applications (ICIEA), 2011 6th IEEE Conference on*, pp. 1943–1947, 2011.

[16] A. Eddahech, O. Briat, R. Chaari, N. Bertrand, H. Henry, and J. M. Vinassa, "Lithium-ion cell modeling from impedance spectroscopy for ev applications," in *Energy Conversion Congress and Exposition (ECCE), 2011 IEEE*, pp. 1449–1453, 2011.

[17] A. Baba and S. Adachi, "State of charge estimation of lithium-ion battery using kalman filters," in *Control Applications (CCA), 2012 IEEE International Conference on*, pp. 409–414, 2012.

[18] A. Di Filippi, S. Stockar, S. Onori, M. Canova, and Y. Guezennec, "Model-based life estimation of li-ion batteries in phevs using large scale vehicle simulations: An introductory study," in *Vehicle Power and Propulsion Conference (VPPC), 2010 IEEE*, pp. 1–6, 2010.

[19] lsqcurvefit, MathWorks. Accessed in September 2013, available at http://www.mathworks.com/help/optim/ug/lsqcurvefit.html.

[20] L. Gao, S. Liu, and R. Dougal, "Dynamic lithium-ion battery model for system simulation," *Components and Packaging Technologies, IEEE Transactions on*, vol. 25, no. 3, pp. 495–505, 2002.

Chapter 4

Impact of Battery Impedance on EV Performance

4.1 Introduction

In this Chapter, the impact of battery impedance on the EV performance is analysed. The importance of active Battery Thermal Management Systems (BTMS) in EVs for range extension and safety consideration is discussed. To demonstrate the impact of battery impedance on EV performance, two Li-Ion batteries are modelled, and their performance are analyzed based on sample drive-cycles of a commercialized electric motorcycle.

The performance of EVs is greatly dependant on the internal impedance of the battery pack. The battery impedance affects the battery voltage based on the SOC and the current being drawn. As discussed in Chapter 1, the inverter fails to continue operating if the terminal voltage drops below the cut-off voltage threshold, hence, the internal impedance can greatly affect the vehicle performance and range [1–4]. Therefore, a battery with minimal internal impedance is desired to achieve better performance of the vehicle.

The battery impedance is extremely sensitive of the operating temperature, which is monitored and controlled by the BTMS. Designing an effective BTMS for an EV is critical as temperature directly affects both the battery lifetime as well as the vehicle range [5–7]. It also affects the safety of EVs which is an important factor in the mass adoption of this technology.

A BTMS consists of two parts, namely, a cooling and a heating system. At low temperatures, the internal impedance of the battery pack is higher due to low activity of chemical reactions and conductivity of electrolyte. This can cause the EV to start or accelerate slowly as the current will be limited by the BMS. Therefore, pre-heating is required to increase the battery temperature to moderate levels (above 5°C) [7–9]. There are several ways to heat the battery as listed below [4, 9–12]:

1. Heating the internal core with alternative current (AC) or direct current (DC) through battery terminals.
2. Heating internal parts of the battery modules by using air, liquid or resistive heating systems.
3. Heating external parts of the battery modules by using air or liquid heating systems. This method is not as efficient as the above listed methods.

At high temperatures (above 50°C), the battery pack can suffer from thermal runaway, a phenomenon where the chemical reactions lose control, resulting in a quick temperature increase, generating heat which causes the self-destruction of the battery [13]. Hence, it is imperative to keep the battery temperature within a moderate range by the thermal management system [9, 13–15]. The deliverable power limit which directly defines the vehicle range is illustrated in Fig. 4.7 as a function of temperature [5, 14].

The BTMS plays a significant role in maximizing the vehicle range and lifetime while minimizing the cost through minimal energy usage. If Toronto is taken as a test city where the minimum temperature can be as low as -30°C on a winter night [16], two scenarios are considered with the EV (200 kg - 9.3 kWh battery pack) parked outside

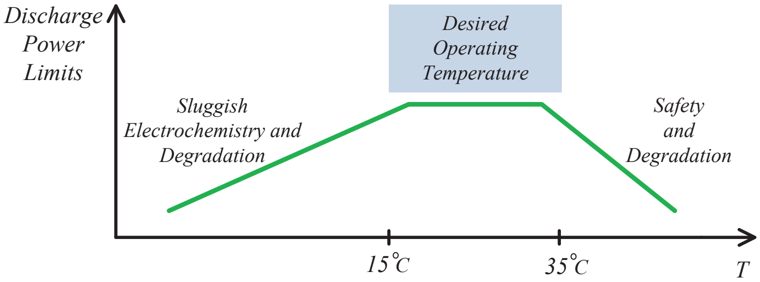

Figure 4.1: Discharge power limit vs. temperature.

and not plugged into the grid. One is when the heater is left on during the night (6 hours) to increase the battery lifetime by maintaining its temperature at moderate levels. If the heater turns on for only two minutes every hour to heat the battery pack to 0°C, it would consume 9 kWh (assuming 100% energy to heat transfer efficiency). Hence, the battery pack would then be almost depleted due to its use by the heater overnight. In the second scenario, the heater is off during the night and the BTMS turns on the heater minutes before the driver starts driving. This would heat up the battery quickly to the desired starting temperature giving it significantly more range, but the battery lifetime would be shortened due to the low battery temperature overnight. As described, a significant trade-off between the first and second scenarios is observed. In the first scenario, the battery lifetime is maximized but the range is severely minimized, whereas, in the second scenario, the range is maximized but the battery lifetime is significantly minimized [3,14].

The BTMS has to find the right balance between achieving the maximum range through either using the battery energy directly to drive the vehicle motor or using the same energy to heat the battery to a higher temperature resulting in lower impedance. In-depth modeling (which provides battery performance and thermal information) are required for the BTMS to find the right balance. The focus of this chapter is to provide an analysis which may be utilized by the BTMS to predict the performance of the vehicle and the battery based on the behaviour of the battery impedance.

4.2 Demonstration of the Impact of Battery Impedance on EV Performance

To demonstrate the effects of battery internal impedance on the performance of EVs, two Li-Ion batteries are modeled, and their performance are analyzed based on real drive-cycles of a commercialized electric motorcycle. The Li-Ion batteries and sample drive-cycles are provided by Brammo, Inc. and are based on an Empulse model motorcycle.

4.2.1 Simulation Setup

The simulation setup for this section consists of three main components, the electric motorcycle, sample drive-cycles and Li-Ion battery cells provided by Brammo Inc. [17].

In 2010, Brammo announced the Empulse water-cooled electric motorcycles (Fig. 4.2) offering a range of 160 km. A list of an Empulse motorcycle specification is provided in Table. 4.1. The maximum speed and mass of the motorcycle is 169 km/h and 212 kg, respectively. The battery pack used in an Empulse model motorcycle is a series combination of seven 14.8 V, 90 Ah BPM battery modules [17]. Each module consists of series and parallel combinations of the 3.7 V, 10 Ah battery cells with the specification provided in Chapter 2.

The urban and freeway drive-cycles discussed in Chapter 2 are based on drive-cycles of an Empulse motorcycle, Fig. 4.3. The average and peak of the cell current are 1 C and 3.5 C for the sample urban drive-cycle. For the sample freeway drive-cycle, the average and peak cell current are 2 C and 4 C, respectively.

Two Li-Ion batteries with the same chemistry and capacity but with different construction types (type A and type B) are provided. The internal impedance of these batteries are slightly different as they are constructed by different vendors. The impedance Nyquist plot of the battery type A and type B are shown in Fig. 4.4(a) and Fig. 4.4(b), respectively. As shown in Fig. 4.4, the internal resistance of the battery type A is higher

Figure 4.2: Empulse motorcycle.

Table 4.1: Empulse Specifications [18]

Motorcycle Parameters	**Value**	**Unit**
Max. Motorcycle Speed, ν_{max}	169	km/h
Motorcycle Mass	212.7	kg
Battery Pack Parameters	**Value**	**Unit**
Number of modules	7	
Pack Capacity (nominal)	9.31	kWh
Pack Voltage, $V_{bt,nom}$	103.6	V
Cycle Life (20% Capacity degradation)	1500	Cycles
Drivetrain Parameters	**Value**	**Unit**
Motor Speed, ω_{max}	8500	rpm
Torque, T_{max}	63	Nm
Power , P_{max}	40	kW

than the battery type B at any temperature. To predict the performance of these cells, they are modeled using the approach discussed in Chapter 3.

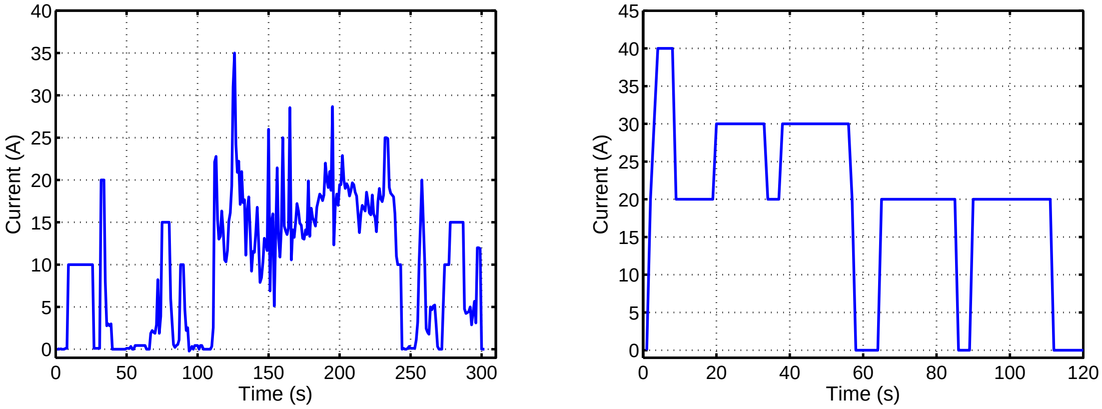

(a) (b)

Figure 4.3: Representative cell current profile for (a) an urban and (b) a freeway drive-cycles in the Empulse motorcycle.

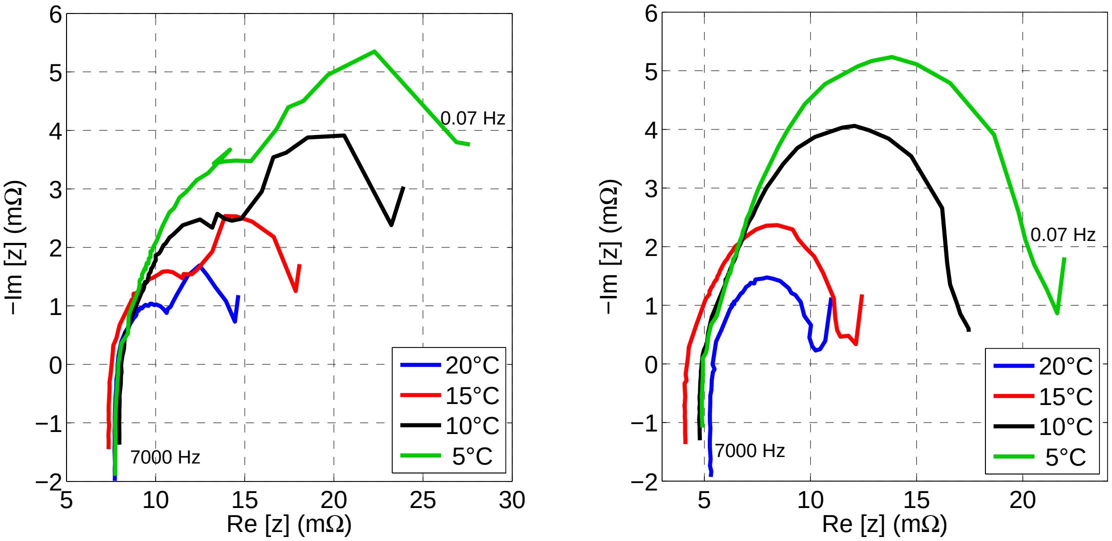

(a) (b)

Figure 4.4: Measured Nyquist curves of cell impedance for (a) type A and (b) type B cells.

4.2.2 Simulation Procedure and Scenarios

Since the electrical model for the two Li-Ion batteries and the real drive-cycles are available, the performance of the battery packs can be compared. The performance of the battery packs is compared, based on the calculated cumulative energy that is delivered until the minimum battery voltage (84 V) is reached. Note that beyond this limit the performance the EV can no longer satisfy the load power and the acceleration would be compromised in the application. Several simulation scenarios are set up to estimate the net drive-cycle energy of the type A and type B battery packs.

The operation of each battery pack in the simulation is terminated if either V_{bt} drops below the battery pack cut-off voltage (84 V), or if the calculated capacity (Ah) reaches the nominal capacity (90 Ah). For the simulation scenarios, three assumptions are considered.

1. Each battery pack consists of identical battery cells with the same electrical, chemical and thermal behaviour.
2. The battery cells used in each battery pack are assumed to be balanced, having the same operating condition such as voltage, current and SOC.
3. The temperature of the battery pack is assumed to be the same as the battery cell temperature. In addition, the battery cell temperature is assumed to be uniform and the thermal effect of the cells on the neighboring cells is ignored.

The simulation scenarios are as follows:

1. Urban drive-cycle

   The urban drive-cycle is extended to provide a one hour current profile with an average current of 1 C (90 A). The performance of the battery packs under the urban drive-cycle at ambient temperature of 0°C (scenario 1) , 5°C (scenario 2), 10°C (scenario 3) and 30°C (scenario 4) are simulated. The voltage and temperature of the battery packs are shown in Fig. 4.5.

2. Freeway drive-cycle

The freeway drive-cycle is extended to provide a 30 minute current profile with an average current of 2C (180 A). The performance of the battery packs under the freeway drive-cycle at ambient temperature of 0°C (scenario 5) , 5°C (scenario 6), 10°C (scenario 7) and 30°C (scenario 8) are simulated. The voltage and temperature of the battery packs are shown in Fig. 4.6.

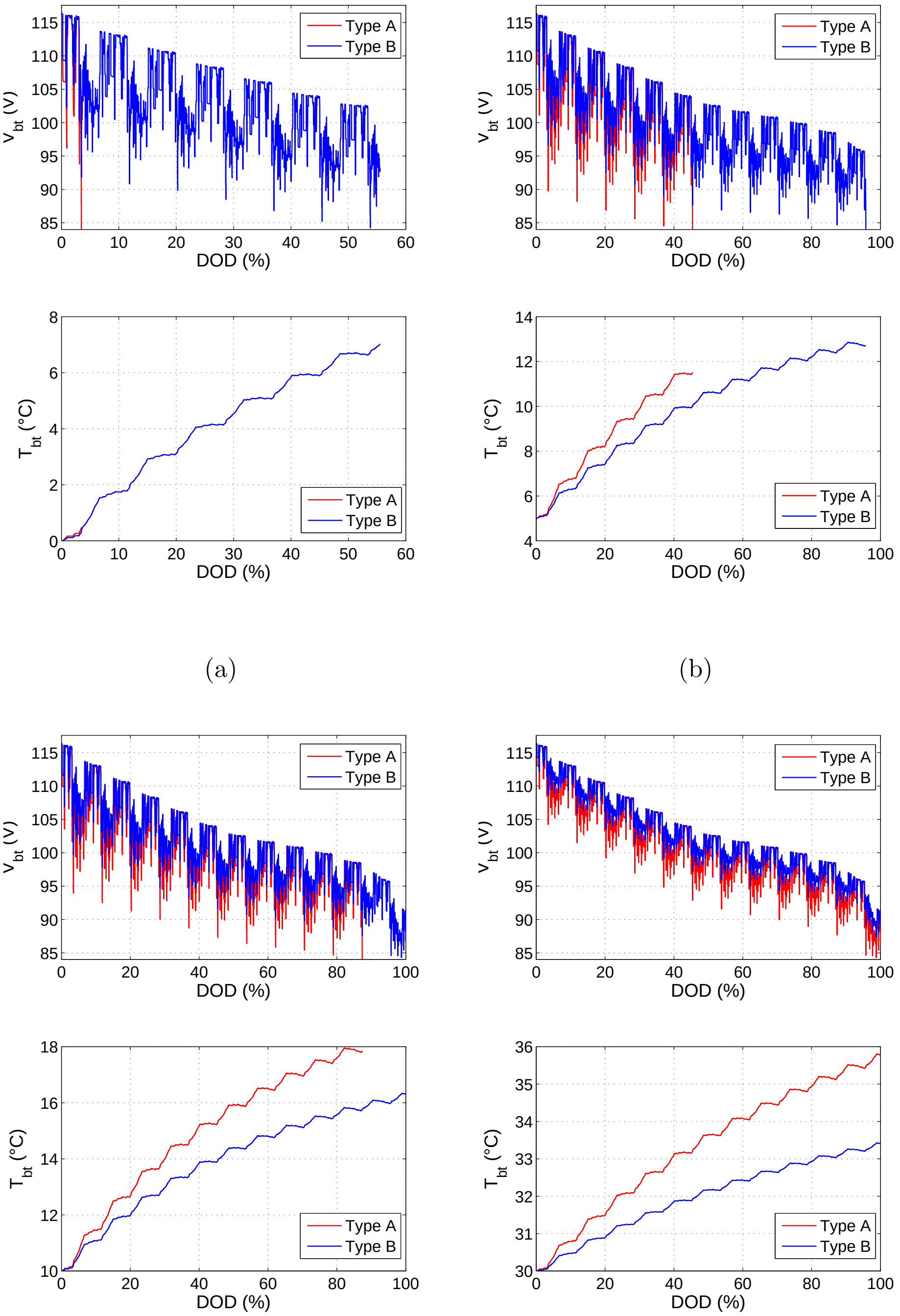

(a)

(b)

(c)

(d)

Figure 4.5: Simulated battery voltage and temperature under urban drive-cycle at ambient temperature of (a) 0°C, (b) 5°C, (c) 10°C and (d) 30°C.

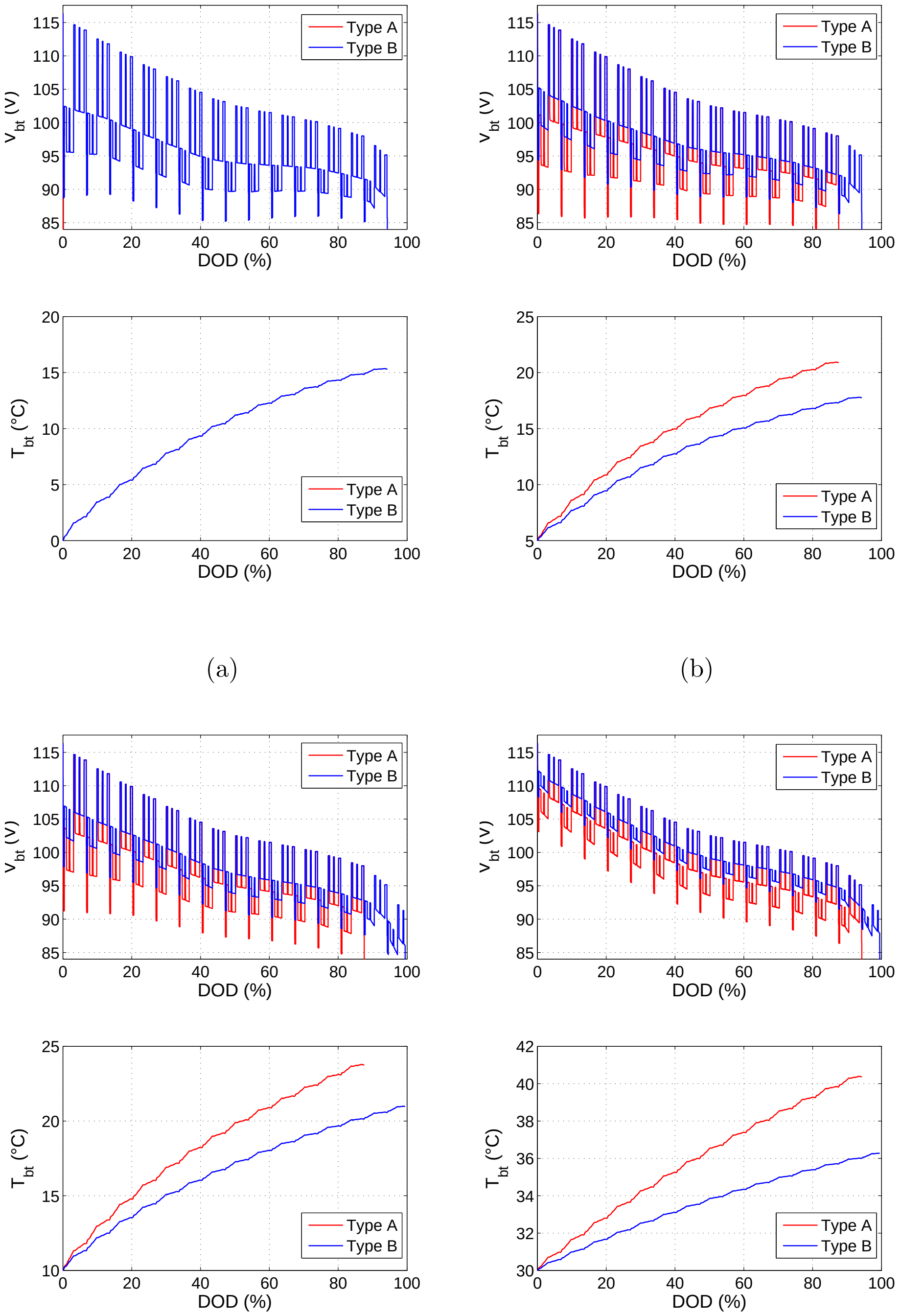

(a) (b)

(c) (d)

Figure 4.6: Simulated battery voltage and temperature under freeway drive-cycle at ambient temperature of (a) 0°C, (b) 5°C, (c) 10°C and (d) 30°C.

4.2.3 Simulation Results and Discussions

The delivered energy by the battery packs in the earlier mentioned scenarios are listed in Table. 4.2. The comparison of the energy delivered by the battery packs at various temperature illustrates the effects of ambient temperature on their performance. Higher ambient temperature results in better performance and higher energy delivery. The lower impedance cell (B) clearly delivers more energy then the higher impedance cell (A).

As the average current of the freeway drive-cycle is 2 times the average current of urban drive-cycle, the temperature rise of the battery in scenario 8 is approximately 2 times the temperature rise in scenario 4, as shown in Fig. 4.5(d) and Fig. 4.6(d).

The effect of self heating is further apparent by comparing the the delivered energy of battery type A in scenario 2 (3.89 kWh) and scenario 6 (7.271 kWh). In both scenarios, the ambient temperature is 5°C. However, the T_{bt} rises to 20°C during the freeway drive-cycle, which enables the battery to operate for a longer duration (see Fig. 4.5(b) and Fig. 4.6(b)).

Based on the simulation results, it is challenging for the BTMS to find the balance between using the battery energy directly to drive the vehicle motor or using the same energy to heat the battery to a higher temperature resulting in lower impedance. For example, if the vehicle with battery type B is on a highway and the ambient temperature is 0°C (scenario 5), the BTMS can turn on the pre-heating system to heat the battery to 5°C (scenario 6), enabling it to deliver 0.218 kWh more to the vehicle. However, the heating system consumes 0.252 kWh to pre-heat the battery from 0°C to 5°C (assuming 100 percent energy to heat transfer efficiency). Therefore, pre-heating the battery is not advantageous as it does not translate into increased range of the vehicle in this particular case.

The envisioned future BTMS system with the on-line self learning ability to optimize the vehicle lifetime and performance is shown in Fig.4.7. The optimization module sets the desired battery pack temperature, and the thermal controller of the system manages the heater or cooler to regulate the battery temperature.

Table 4.2: Delivered Energy in Simulation Scenarios

	Battery Type	Ambient Temperature (°C) 0	5	10	30
Urban Drive Cycle					
Delivered Energy(kWh)	A	0.172	3.890	7.500	8.883
	B	4.874	8.211	8.824	9.066
Freeway Drive Cycle					
Delivered Energy (kWh)	A	0.012	7.271	7.419	8.214
	B	7.823	8.0411	8.637	8.955

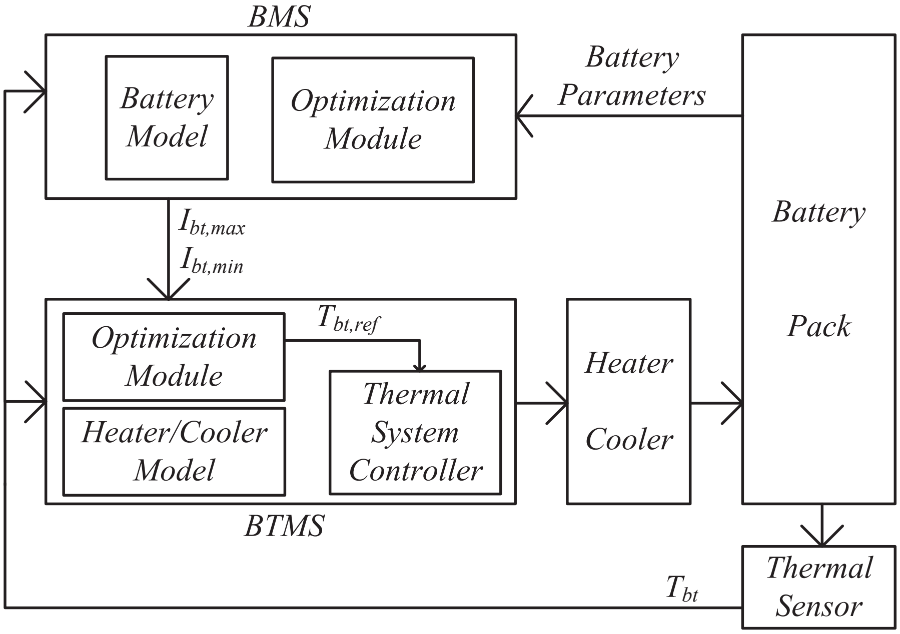

Figure 4.7: Control circuit for BTMS.

4.3 Chapter Summary and Conclusion

In this Chapter, the impact of battery impedance on the performance of EVs is discussed. Batteries with minimal internal impedance are desired for better vehicle performance. The effects of temperature on the battery impedance and the vehicle performance are also covered. At low temperatures, the battery has sluggish behaviour resulting in higher battery impedance and lower vehicle range. However, at high temperatures, the battery overheats which can shorten its lifetime. Therefore, the BTMS which controls and monitors the battery temperature, plays an important role in range and lifetime extension.

To demonstrate the effect of battery impedance on the vehicle range, an analysis based on a simulation setup is provided. The performance of two Li-Ion battery types under sample urban and freeway drive-cycles at various ambient temperatures are evaluated. Based on the simulation results, the battery with lower internal impedance can deliver significantly more energy before reaching under-voltage.

When operating in cold climates, it is observed that the BTMS faces challenges to strike the balance to achieve higher vehicle range by either using the battery energy directly to drive the motor or using the same energy to heat the battery to a higher temperature, resulting in higher range. Therefore, the detailed battery model provided in this thesis can be utilized by the BTMS to find the optimum real-time operating battery temperature for better vehicle performance.

References

[1] D. V. Do, C. Forgez, K. El-Kadri-Benkara, and G. Friedrich, "Impedance observer for a li-ion battery using kalman filter," *Vehicular Technology, IEEE Transactions on*, vol. 58, no. 8, pp. 3930–3937, 2009.

[2] G. Liu, M. Ouyang, L. Lu, L. Xu, and J. Li, "Online monitoring of lithium-ion battery aging effects by internal resistance estimation in electric vehicles," in *Control Conference (CCC), 2012 31st Chinese*, pp. 6851–6855, 2012.

[3] C. Mi, B. Li, D. Buck, and N. Ota, "Advanced electro-thermal modeling of lithium-ion battery system for hybrid electric vehicle applications," in *Vehicle Power and Propulsion Conference, 2007. VPPC 2007. IEEE*, pp. 107–111, 2007.

[4] T. Mller, "Lithium ion battery automotive applications and requirements," in *Battery Conference on Applications and Advances, 2002. The Seventeenth Annual*, pp. 113–118, 2002.

[5] A. Pesaran, M. Keyser, G. Kim, S. Santhanagopalan, and k. Smith, "Tools for designing thermal management of batteries in electric drive vehicles," in *Large Lithium Ion Battery Technology and Application Symposia, Advanced Automative Battery Conference*, 2013.

[6] A. Pesaran and M. Keyser, "Thermal characteristics of selected ev and hev batteries," in *Annual Battery Conference: Advances and Applications*, 2001.

[7] H.-S. Song, J.-B. Jeong, B.-H. Lee, D.-H. Shin, B.-H. Kim, T.-H. Kim, and H. Heo, "Experimental study on the effects of pre-heating a battery in a low-temperature environment," in *Vehicle Power and Propulsion Conference (VPPC), 2012 IEEE*, pp. 1198–1201, 2012.

[8] H.-S. Song, J.-B. Jeong, B.-H. Lee, D.-H. Shin, B.-H. Kim, T.-H. Kim, and H. Heo, "Experimental study on the effects of pre-heating a battery in a low-temperature environment," in *Vehicle Power and Propulsion Conference (VPPC), 2012 IEEE*, pp. 1198–1201, 2012.

[9] C. Alaoui, "Solid-state thermal management for lithium-ion ev batteries," *Vehicular Technology, IEEE Transactions on*, vol. 62, no. 1, pp. 98–107, 2013.

[10] A. Pesaran, A. Vlahinos, and T. Stuart, "Cooling and preheating of batteries in hybrid electric vehicles," in *The 6th ASME-JSME Thermal Engineering Joint Conference*, 2003.

[11] "Nissan leaf." Nissan, 2013 Nissan Leaf. Accessed in September 2013, available at http://www.nissan.ca/ms/leaf20/en/index.html.

[12] "Tesla." Tesla Motors, Tesla Module S. Accessed in September 2013, available at http://www.teslamotors.com.

[13] C. Sen and N. Kar, "Battery pack modeling for the analysis of battery management system of a hybrid electric vehicle," in *Vehicle Power and Propulsion Conference, 2009. VPPC '09. IEEE*, pp. 207–212, 2009.

[14] K. Qian, C. Zhou, Y. Yuan, and M. Allan, "Temperature effect on electric vehicle battery cycle life in vehicle-to-grid applications," in *Electricity Distribution (CICED), 2010 China International Conference on*, pp. 1–6, 2010.

[15] Y. Chen, L. Song, and J. Evans, "Modeling studies on battery thermal behaviour, thermal runaway, thermal management, and energy efficiency," in *Energy Conversion Engineering Conference, 1996. IECEC 96., Proceedings of the 31st Intersociety*, vol. 2, pp. 1465–1470 vol.2, 1996.

[16] "Toronto waether overview." The Weather Network, Statistics. Accessed in September 2013, available at http://www.theweathernetwork.com/forecasts/statistics/cl6158350/caon0696.

[17] Brammo, Inc. Accessed in August 2013, available at http://www.brammo.com/home/.

[18] "2013 empulse and empulse r owner's manual." Brammo, datasheet. Accessed in August 2013, available at http://www.brammo.com/home/.

Chapter 5

Conclusion

5.1 Thesis Summary and Contribution

The focus of this work is on the design of a battery cell testing platform and Lithium-Ion (Li-Ion) battery modeling for EVs. A novel regenerative and programmable cell testing platform is developed as the suitable choice to test the automatize grade batteries under real-world drive-cycle profiles. A novel battery modeling approach is proposed to accurately predict the battery performance. The proposed model is intended to be implemented in real-time BMS systems to further improve the vehicle performance. In addition, the model is utilized to assess the long-term impact of battery impedance on performance of EVs under real-world drive-cycles.

The novel contributions of this work include:

- Design of a novel cell cycler architecture to provide a fast, regenerative and programmable cell cycling platform utilizing inverters and LICs;
- Implementation of the proposed architecture by utilizing grid-tie inverter for power delivery to the grid and LICs for high efficiency and system stability;
- Providing the cell cycler system with a modular design to provide expansion flexi-

bility to the cycling platform;

- Design of a novel battery modeling approach to accurately predict the battery performance by dynamically updating model parameters based on the battery temperature and SOC; and
- Development of a simulation setup to quantify the impact of battery impedance on performance of EVs under real-world drive-cycles.

The proposed 300 W - 5 V cell cycler is designed utilizing an interleaved two phase buck and an interleaved two phase boost converters. Two- phase interleaved architecture is used to achieve higher efficiency. The cycler system is implemented with the switching frequency of 200 kHz which is capable tracking dynamic current of up to 8 A/ms.

Furthermore, in Chapter 3, a modelling example of a commercialized Li-Ion battery is presented to demonstrate the proposed approach. The model parameters are extracted based on impedance and thermal measurements while considering the self-heating of the battery. The accuracy of the model is verified by comparisons of the simulation and experimental results under a constant and the urban drive-cycle current profiles. It is shown that the battery temperature rises by 11°C under 2 C discharge current at room temperature. Therefore, the benefit of including self heating process to the model is justified.

In Chapter 4, a simulation setup with various scenarios is provided to quantitatively demonstrate the impact of battery impedance on EV performance. Simulation evaluation of the performance of two automatize grade Li-Ion batteries in various scenarios are presented. The comparisons between battery performance in different simulation scenarios show the superior benefit of low battery impedance when the battery type B can deliver 50 times more energy than battery type A under Urban drive-cycle in 0°C. The indirect effects of temperature on the vehicle performance is also observed by comparing the performance of battery packs in various temperatures.

5.2 Future Work

Based on the presented research work in this thesis, the following suggestions are provided for further explorations:

- Using the multi-channel testing platform, the effect of ambient temperature, average current and current profiles on life time of Li-Ion batteries can be analyzed by performing capacity measurements tests on the batteries after a certain number of cycles.

- The battery model can be further improved by integrating the effect of degradation. The model parameters can be measured overtime (at different number of cycles). The model parameters can then be updated dynamically based on SOC, battery temperature and degradation.

- The performance of the battery pack, discussed in Chapter 4, can be improved by considering mismatches among the battery cells and the non-uniformity of the temperature distribution in the cell, module and battery pack. However, this can further complicate the calculations that should be done by the BTMS in real-time.